Precambrian Research 310 (2018) 391–406

Contents lists available at ScienceDirect

Precambrian Research

journal homepage: www.elsevier.com/locate/precamres

Neoproterozoic $^{40}Ar/^{39}Ar$ mica ages mark the termination of a billion years of intraplate reworking in the Capricorn Orogen, Western Australia

Agnieszka M. Piechocka[a,*], Stephen Sheppard[a,b], Ian C.W. Fitzsimons[a], Simon P. Johnson[c], Birger Rasmussen[d], Fred Jourdan[a]

[a] School of Earth and Planetary Sciences, Curtin University, Kent Street, Bentley, WA 6102, Australia
[b] Prime Geological Mapping, PO Box 3014, Carlisle South, WA 6101, Australia
[c] Geological Survey of Western Australia, 100 Plain Street, East Perth, WA 6004, Australia
[d] School of Earth Sciences, The University of Western Australia, Nedlands, WA 6009, Australia

ARTICLE INFO

Keywords:
Intraplate orogeny
$^{40}Ar/^{39}Ar$ geochronology
U-Pb xenotime geochronology
Neoproterozoic
Capricorn orogen
West Australian Craton

ABSTRACT

The tectonic history of the Proterozoic Capricorn Orogen, Western Australia, records complex intraplate reworking lasting nearly one billion years. Although the Paleo-Mesoproterozoic reworking history is well defined in the crystalline basement of the Gascoyne Province, at the western end of the orogen, the younger reactivation history remains unclear. Four reworking events affected the orogen at 1820–1770 Ma, 1680–1620 Ma, 1320–1170 Ma, and 1030–900 Ma. These events were succeeded by a breakout in predominantly dextral strike-slip reactivation of major shear zones across the Gascoyne Province. Currently, the age of this reactivation is constrained by only one date of c. 570 Ma from a single shear zone, but field relationships imply that some of the shear zones must be older than a suite of c. 755 Ma dolerite dykes. In order to constrain the age of fault and shear zone reactivation we obtained new $^{40}Ar/^{39}Ar$ dates for mica and *in situ* SHRIMP U-Pb dates for xenotime within shear zones. Our results when combined with previously published data, show that reactivation occurred between 920 and 830 Ma. These dates overlap with the youngest reworking event, the 1030–900 Ma Edmundian Orogeny. Furthermore, Neoproterozoic U-Pb phosphate ages are known from the bounding cratons and faulting within the adjacent Mesoproterozoic sedimentary basins suggest this event is of regional significance. In contrast to previous suggestions that this Neoproterozoic reactivation was the result of a collision from the west, we propose that it reflects north–south compression that caused dextral strike-slip fault reactivation in the north and exhumation of the southern part of the orogen.

1. Introduction

Intraplate orogens are less common than orogens at plate margins but their significance in tectonics is increasingly recognized (e.g., Aitken et al., 2009; Raimondo et al., 2010, 2014). Intraplate orogens are highly susceptible to repeated tectonic activity which is commonly considered to be a far-field response to events at plate margins (e.g., Aitken et al., 2013; Raimondo et al., 2014; Dyksterhuis and Müller, 2008). The Petermann and Alice Springs orogenies in central Australia and the Tien Shan orogen in central Asia are regarded as archetypal examples of compressional intraplate tectonics, all being characterised by thickening and substantial exhumation (Aitken et al., 2009; Raimondo et al., 2014). However, it is unlikely that these orogenies reflect the full range of behaviour in intraplate settings.

The Capricorn Orogen is a zone ~1000 km long and 500 km wide that comprises the deformed margins of two Archean cratons (the Pilbara Craton in the north and Yilgarn Craton in the south) and intervening Proterozoic granitic and metasedimentary rocks of the Gascoyne Province, overlain by variably deformed Paleo- to Mesoproterozoic sedimentary basins (Cawood and Tyler, 2004) (Fig. 1). These rocks record the two-stage assembly of the Pilbara and Yilgarn cratons to form the larger West Australian Craton. First, the Pilbara Craton collided with the Glenburgh Terrane during the c. 2200 Ma Ophthalmian Orogeny, which was followed by the subsequent collision of the Pilbara Craton-Glenburgh Terrane with the Yilgarn Craton at c. 1950 Ma during the Glenburgh Orogeny (Cawood and Tyler, 2004; Johnson et al., 2011; Occhipinti et al., 2004). After assembly, the orogen remained susceptible to reworking and reactivation, recording a prolonged tectonothermal history spanning over one billion years. The protracted tectonic history involved four episodes of tectonothermal reworking (Korhonen et al., 2017; Sheppard et al., 2005, 2007, 2010b), followed by one or more poorly constrained reactivation events, all of

* Corresponding author.
E-mail address: nishka.piechocka@postgrad.curtin.edu.au (A.M. Piechocka).

https://doi.org/10.1016/j.precamres.2018.04.006
Received 16 February 2018; Received in revised form 16 March 2018; Accepted 5 April 2018
Available online 06 April 2018

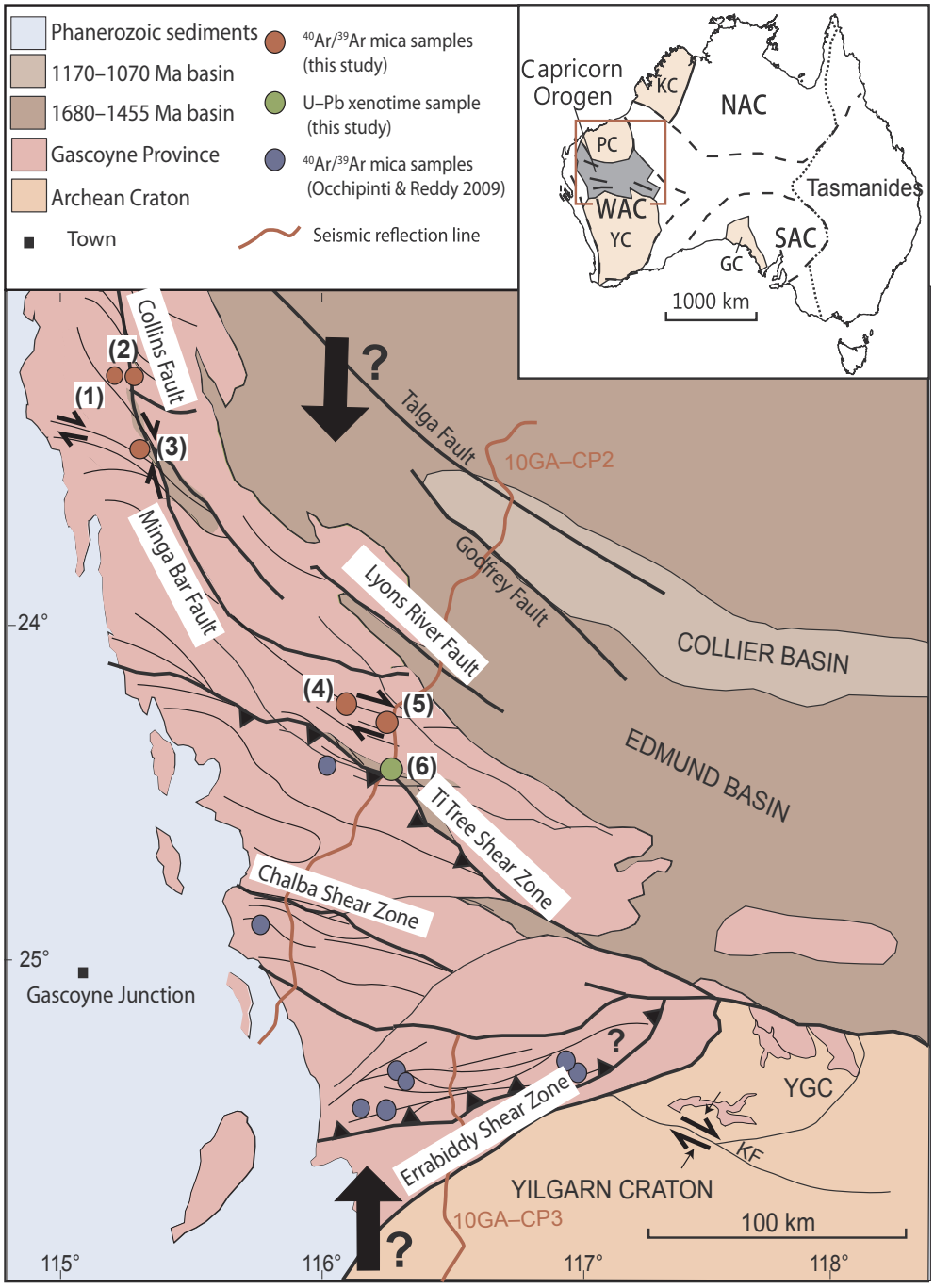

Fig. 1. Regional geological map of the Gascoyne Province, Capricorn Orogen. The large black arrows indicate the suggested north–south compression. Numbers in brackets relate to sample localities detailed in Table 1. (1) GSWA 216533; (2) GSWA 216540B; (3) GSWA 195890B and D and E; (4) GSWA 183294; (5) GSWA 183295; (6) GSWA 149,009 & 149010. KF—Kerba Fault (Reddy and Occhipinti, 2004), YGC—Yilgarn Gneiss Complex, YC—Yilgarn Craton, PC—Pilbara Craton, WAC—West Australian Craton, KC—Kimberley Craton, NAC—North Australian Craton, GC—Gawler Craton, SAC—South Australian Craton. (Modified after Johnson et al., 2017).

which are best recorded in the Gascoyne Province at the western end of the orogen. The youngest elements of the orogen are very low-grade metasedimentary rocks of the 1680–1465 Ma Edmund Basin and the 1170–1070 Ma Collier Basin.

The Gascoyne Province comprises several southeast-trending structural and metamorphic zones each recording a unique history of reworking (Sheppard et al., 2010b). Although the Paleo-Mesoproterozoic reworking history is well constrained (Korhonen et al., 2017; Sheppard et al., 2005, 2007, 2010b) the history of Neoproterozoic reactivation and uplift is almost entirely unknown. Poorly constrained total fusion $^{40}Ar/^{39}Ar$ mica dates of c. 920–860 Ma, obtained from the southern Errabiddy Shear Zone, were interpreted to represent cooling after a regional greenschist reworking event (Occhipinti and Reddy, 2009). The youngest known reactivation event, the c. 570 Ma Mulka Tectonic Event (Bodorkos and Wingate, 2007) identified by *in situ* $^{40}Ar/^{39}Ar$ mica dating, is known from one shear zone in the southern province, the Chalba Shear Zone (Fig. 1). The Chalba Shear Zone is characterised by dextral strike-slip kinematics and cross cuts c. 755 Ma dykes of the Mundine Well Dolerite Suite (Wingate and Giddings, 2000). Other undated shear zones in the area show the same kinematics and offset the c. 755 Ma dolerites suggesting that they also belong to the Mulka Tectonic Event. However, field relationships show that some shear zones are cut by the c. 755 Ma dolerite dykes suggesting that there was also an older reactivation event. In the northern half of the orogen, numerous shear zones with dextral kinematics cut metasedimentary rocks of the 1680–1465 Ma Edmund Group and probably the 1170–1070 Ma Collier Group, but the age of this faulting and shear zone reactivation event is unknown.

The focus of this study is to determine the age and cause of the low-temperature reactivation of shear zones in the northern Capricorn

Table 1
Summary of field data and sample details from the Gascoyne Province, Capricorn Orogen.

Sample ID	Latitude (N)	Longitude (E)	Rock type	Structures	Shear Zone	$^{40}Ar/^{39}Ar$ age (Ma)	$^{207}Pb^*/^{206}Pb^*$ (Ma)
GSWA 149,009 (6)	−24° 22′ 12.91	116° 04′ 04.03	Laminated siltstone	Bedding 305°/76° NE (35°)	Ti Tree Shear Zone		891 ± 26 (1σ)
GSWA 149,010 (6)	−24° 21′ 59.33	116° 04′ 01.36	Silicified mudstone	Cleavage 106°/80° SW (196°)	Ti Tree Shear Zone		893 ± 25
GSWA 183,294 (4)	−24° 20′ 27.81	116° 17′ 24.73	Quartz-muscovite mylonite	Lineation 25°/141° 1820–1770 Ma Metamorphic foliation 141°/85° WSW	Shears within the Minnie Creek Batholith	882 ± 3	
GSWA 183,295 (5)	−24° 19′ 25.22	116° 08′ 42.01	Quartz–muscovite mylonite	Lineation 30°/112° 1820–1770 Ma Metamorphic foliation 304°/87° NE	Shears within the Minnie Creek Batholith	882 ± 3	
GSWA 195890B (3)	−23° 31′ 33.13	115° 25′ 03.46	Porphyritic muscovite-biotite monzogranite	Lineation 0°/140° and 0°/160° Vertical mylonite sets at 140° and 160° 1680–1620 Ma Metamorphic foliation 140°/85° WSW	2 km west of Collins Fault	862 ± 4*	
GSWA 216540B (2)	−23° 16′ 47.97	115° 21′ 06.19	Leucocratic muscovite–biotite monzogranite	Vertical mylonites trend at 160° 1680–1620 Ma Metamorphic foliation 190°/90°	Collins Fault	898 ± 3*	
GSWA 216,533 (1)	−23° 16′ 48.42	115° 20′ 37.93	Biotite-garnet schist	1680–1620 Ma Metamorphic foliation 151°/30° WSW	0.8 km west of the Collins Fault	908 ± 3	
GSWA 216,533 (1)	−23° 16′ 48.42	115° 20′ 37.93	Biotite–garnet schist	1680–1620 Ma Metamorphic foliation 151°/30° WSW	0.8 km west of the Collins Fault	918 ± 3	
GSWA 195890D (3)	−23° 31′ 33.13	115° 25′ 03.46	Porphyritic muscovite-biotite monzogranite	Lineation 0°/140° and 0°/160° Vertical mylonite sets at 140° and 160° 1680–1620 Ma Metamorphic foliation 140°/85° WSW	2 km west of Collins Fault	1642 ± 7	
GSWA 195890E (3)	−23° 31′ 33.13	115° 25′ 03.46	Porphyritic muscovite-biotite monzogranite	Lineation 0°/140° and 0°/160° Vertical mylonite sets at 140° and 160° 1680–1620 Ma Metamorphic foliation 140°/85° WSW	2 km west of Collins Fault	1639 ± 8	

Notes: Numbers in brackets, in sample ID column, refer to locations in Fig. 1 in the main body text.
Planar structures are quoted as srike/dip.
Pb* indicates radiogenic Pb (i.e. corrected for common Pb).
$^{207}Pb^*/^{206}Pb^*$ xenotime weighted mean dates are reported with 95% confidence limits unless otherwise specified.
$^{40}Ar/^{39}Ar$ weighted means reported at 2 sigma level.
*Indicates a mini plateau age.

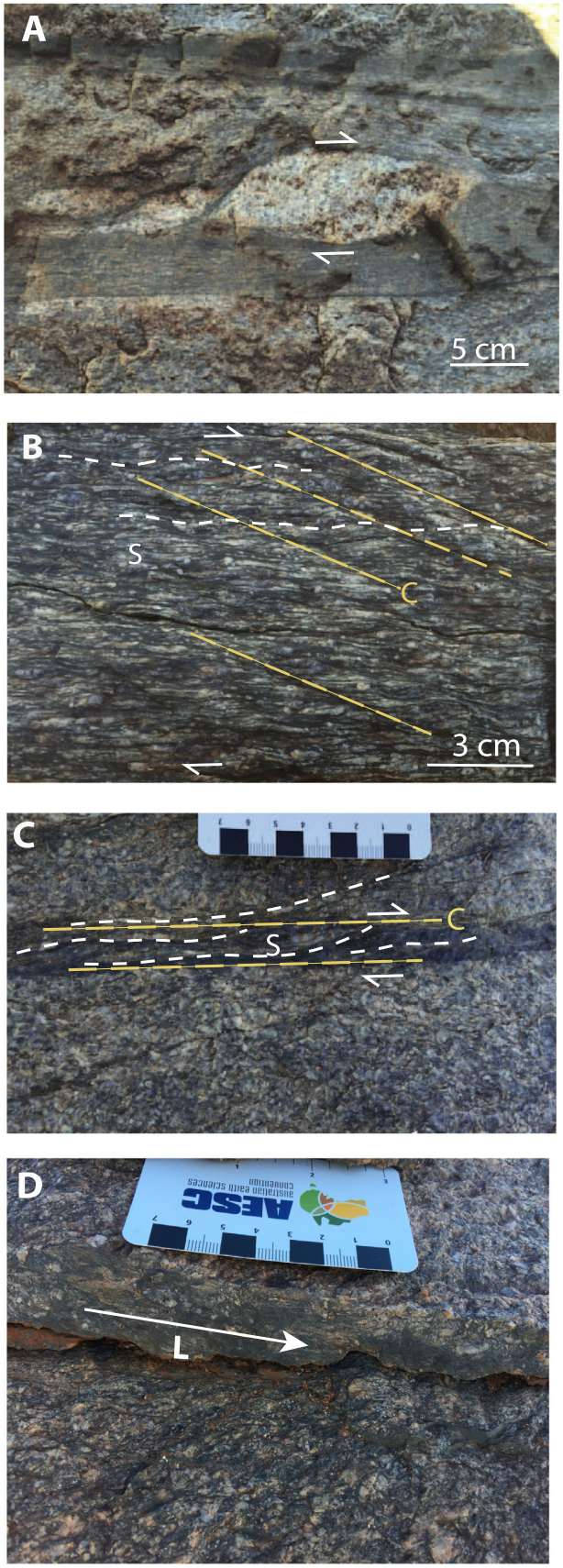

Fig. 2. A: Granitic clast (composed of feldspar and quartz) with dextral sigma tails within a ~15 cm-wide mylonite zone (Collins Fault, locality 2, GSWA 216540B). B: Extensional crenulation cleavage defined by recrystallised biotite and feldspar augen within a porphyritic biotite rich monzogranite, locality within 80 m of sample GSWA 216540B (Collins Fault, locality 2). C: Well-developed C-S fabric in the porphyritic muscovite-biotite monzogranite showing a lower strain rate and less deformation away from the major Collins Fault (Locality 3 and GSWA 195890). D: Subhorizontal lineation within a mylonite zone at Locality 3. For localities refer to Fig. 1.

Orogen by integrating $^{40}Ar/^{39}Ar$ mica and U-Pb xenotime geochronology. Dating low-grade hydrothermal fluid flow within major faults may be achieved by U-Pb phosphate geochronology (e.g.,Rasmussen et al., 2007, 2010) but preliminary dating of one major shear zone, in the northern Gascoyne Province, using monazite yielded a Paleoproterozoic age (unpublished data) which is likely to date the host rock rather than the reactivation. Although, no datable xenotime was identified in the northern shear zones we were able to date a central shear zone using U-Pb xenotime geochronology. Therefore we turned to $^{40}Ar/^{39}Ar$ mica geochronology to date the low-grade fault reactivation in the Gascoyne Province. Our study also demonstrates that the reactivation event dated here does not involve substantial crustal thickening or exhumation, unlike other key examples of compressional intraplate orogens.

2. Intraplate reworking and reactivation in the Gascoyne Province

2.1. Reworking

The earliest episode of reworking occurred at 1820–1770 Ma during the Capricorn Orogeny and is marked by the emplacement of voluminous felsic magmatic rocks and extensive deformation, mostly at low to medium metamorphic grade (Sheppard et al., 2010a). This event has the largest metamorphic and magmatic footprint of all the intraplate reworking events to have affected the orogen; igneous rocks, metamorphic assemblages and structures attributed to the Capricorn Orogeny span the entire orogen, from the Errabiddy Shear Zone in the south to north of the Collins Fault (Fig. 1). The Capricorn Orogeny was followed by the 1680–1620 Ma Mangaroon Orogeny, which is characterised by voluminous felsic magmatism and complex deformation and medium- to high-grade metamorphism (< 750 °C and < 6 kbar; Sheppard et al., 2005). The Mangaroon Orogeny reworked a smaller portion of the Gascoyne Province with only the central and northern parts affected (i.e., from the Chalba Shear Zone to the Collins Fault). The next event was the Mutherbukin Tectonic Event at 1320–1170 Ma, which comprised deformation and metamorphism at > 650 °C and 4.4–7 kbar (Korhonen et al., 2017), but without magmatism, affecting the central parts of the orogen only (i.e., between the Ti Tree Shear Zone and Chalba Shear Zone). The youngest reworking event, the Meso–Neoproterozoic Edmundian Orogeny 1030–950 Ma (Sheppard et al., 2007), is restricted to a 20 km-wide structural corridor south of the Ti Tree Shear Zone (Fig. 1). This orogeny was characterised by local deformation and greenschist to amphibolite facies metamorphism (500–550 °C and 3–4 kbar) from 1030 to 990 Ma and leucocratic magmatism at 950 Ma (Sheppard et al., 2007). The age of leucocratic magmatism was further constrained by Piechocka et al. (2017) from 1006 to 899 Ma, showing that magmatism persisted for c. 90 million years and providing a new minimum age constraint for the Edmundian Orogeny at 900 Ma.

2.2. Reactivation

The youngest known events in the Capricorn Orogen involve the reactivation of a series of major, sub-parallel, predominantly low-grade shear zones and faults (Fig. 1), many of which are crustal-scale structures related to the assembly of the West Australian Craton (Johnson

et al., 2013). However, the timing of this reactivation is poorly constrained. The youngest known reactivation event was identified by a c. 570 Ma $^{40}Ar/^{39}Ar$ mica date from a dextral shear zone in the central part of the Gascoyne Province that cross-cuts and offsets dolerite dykes of the c. 755 Ma Mundine Well Dolerite Suite (Bodorkos and Wingate, 2007; Wingate and Giddings, 2000). However, other cross-cutting relationships imply that most of the reactivation is older because shear zones and faults that affect Mesoproterozoic sedimentary rocks of the Edmund Basin and, possibly the Collier Basin (Cutten et al., 2016) are themselves cut by c. 755 Ma dolerite dykes (Wingate and Giddings, 2000). These field relationships suggest the presence of another reactivation event between c. 1465 and 755 Ma in the Capricorn Orogen.

3. Characteristics of fault and shear zone reactivation and sample details

In the Gascoyne Province the major faults and shear zones, as well as their ancillary structures, are sub-vertical at surface and some carry a shallow-plunging (0–30°) stretching lineation (sub-horizontal in the north and plunging up to 30° in the central parts of the province), implying dominantly strike-slip deformation with a minor component of uplift in the centre of the province (Table 1). Regional-scale map patterns of anastomosing faults, as well as local shear sense indicators (sigma and delta porphyroclasts, S–C fabrics and asymmetric extensional shear bands; Fig. 2A–C; Hanmer and Passchier, 1991), imply an overall dextral sense of shear, although the style of deformation varies across the province.

3.1. The northern Gascoyne Province (Collins Fault)

In the northern part of the Gascoyne Province (i.e., Collins Fault) deformation is partitioned mainly into discrete, 1–50 mm-wide, anastomosing zones of mylonite within medium- to coarse-grained granitic rocks (Fig. 3A). The mylonite zones commonly show millimetre- to centimetre-scale offsets, with the production of early ductile S–C fabrics that are overprinted by brittle cataclastic textures. Samples GSWA 216540B and 195890B and D–E, which are representative of these thin mylonites, were collected from two different localities (Fig. 1; Table 1) showing different levels of strain (Fig. 2A and C) for $^{40}Ar/^{39}Ar$ mica dating. Horizontal lineations (Fig. 2D) and shear sense indicators at the GSWA 195890 sample locality (Table 1) suggest dextral strike-slip movement.

Sample GSWA 216540B is a deformed muscovite–biotite metamonzogranite comprising K-feldspar, quartz, plagioclase and muscovite with 5% mafic minerals biotite, chlorite (2%) and accessory zircon and monazite. The quartz is recrystallised and shows undulose extinction. The well-defined foliation is characterised by aligned recrystallised quartz and elongate muscovite crystals. Zones of mylonitisation are characterised by fine-grained recrystallised muscovite, with the occasional larger primary muscovite (Fig. 3E and F). Feldspar porphyroclasts are elongate and show sigma tails with a dextral sense of shear. There is minimal preservation of primary igneous textures (in contrast to GSWA195890 below) with sparse relatively undeformed K-feldspar phenocrysts. Sericite and perthite are indicative of post magmatic alteration.

Sample GSWA 195890 (B and D–E) is a medium-grained muscovite–biotite metamonzogranite that in parts contains a well-developed S–C fabric. The metamonzogranite shows variation in strain across the outcrop with zones of mylonitisation (biotite), quartz veining and brecciation and zones with preserved igneous textures. The typical mineral assemblage consists of K-feldspar, quartz, muscovite and plagioclase with mafic minerals making up around 25% and includes biotite, chlorite (10–15%) iron oxides with accessory fluorite, zircon and monazite. The preserved igneous muscovite (as mildly deformed porphyroclasts) occur as large crystals up to ~4 mm in length and the biotite forms the very fine-grained matrix (Fig. 3A–D).

Deformation is also partitioned into laterally discontinuous, compositionally weaker zones 0.3–10 m wide. One sample from a ~30 cm-wide zone of strongly deformed, biotite–garnet gneiss (sample GSWA 216533) with 1–5 cm-wide, discontinuous leucocratic veins (Fig. 4B) was collected for $^{40}Ar/^{39}Ar$ mica dating. Sample GSWA 216533 is defined by a well-developed gneissic fabric comprised of alternating domains of elongate biotite with minor elongate muscovite; recrystallised quartz; and, recrystallised very-fine grained muscovite. The mineral assemblage is garnet (15%), biotite (25%), quartz (20%), muscovite (20%), chlorite (9%), epidote (8%), opaques (2%), and plagioclase (1%). The inclusions in the garnet cores consist of quartz, muscovite and biotite, with epidote in the garnet rims. The biotite ranges in pleochroism from light tan colour to a medium green-brown colour. The biotite porphyroblasts that occur within the very fine-grained muscovite layer typically show two internal fabrics (Fig. 3G and H). The fabric shows either an oblique orientation to the main foliation or is parallel to the foliation. Muscovite occurs as millimetre-sized tabular crystals intergrown with the biotite. Recrystallized muscovite forms the very fine-grained matrix. Some of the quartz and biotite show sigma tails with dextral kinematics. Late chlorite alteration post-dates the peak metamorphic assemblage.

3.2. The central Gascoyne Province (Ti Tree shear Zone)

In the central part of the province (north of the Ti Tree Shear Zone) discrete, discontinuous zones of quartz–muscovite mylonite up to 5 m wide are developed in coarse-grained granitic rocks (Fig. 4C). These mylonites are associated with ancillary structures related to major faults. The quartz mylonites are steeply dipping with shallowly-plunging east–southeast stretching lineations and locally contain well-developed S–C fabrics that indicate dextral strike-slip movement. Two samples (GSWA 183284 and 183285) were collected for $^{40}Ar/^{39}Ar$ mica dating from typical quartz-muscovite mylonite zones. Shallowly plunging lineations (Fig. 4C) within the quartz-muscovite mylonite zones (Table 1) indicate predominantly strike-slip movement with minor uplift of the southern side.

The Ti Tree Shear Zone is interpreted to be a major crustal structure (Johnson et al., 2013) with evidence for multiple Proterozoic movements (Korhonen et al., 2017). At the southeastern end of the shear zone phyllites of the Edmund Group have been strongly silicified (Fig. 4D) and contain a steeply dipping cleavage and steeply plunging intrafolial folds with axial surfaces parallel to the cleavage. Two quartz phyllite samples (GSWA 149009 and 149010, ~400 m apart) were collected for U-Pb xenotime geochronology.

A summary of all samples used in this study and location details are provided in Table 1.

4. Geochronology methodology

4.1. $^{40}Ar/^{39}Ar$ mica geochronology

$^{40}Ar/^{39}Ar$ geochronology was carried out on single mica crystals from mineral separates of seven samples; muscovite was dated from six of these samples (GSWA 183294, 183295, 195890D–E, 216533 and 216540B) and biotite from two of them (samples GSWA 195890B and 216533). Muscovite and biotite crystals, ranging from 355 to 125 µm size fractions, were washed and dried and then hand-picked under a binocular stereomicroscope. Only unaltered and transparent grains were chosen. The best looking grains were selected and were irradiated for 40 h in the Oregon State University nuclear reactor in central position during two separate irradiations (I22 in April–July 2016 and I23 in November 2016–February 2017). For both irradiations the best grains (i.e., transparent with pearly lustre) were loaded in two separate discs that were Cd-shielded (to minimize undesirable nuclear interference reactions). I23 included a fully calibrated Fish Canyon sanidine (FCs) standard, for which an age of 28.294 Ma (± 0.13%; Renne et al.,

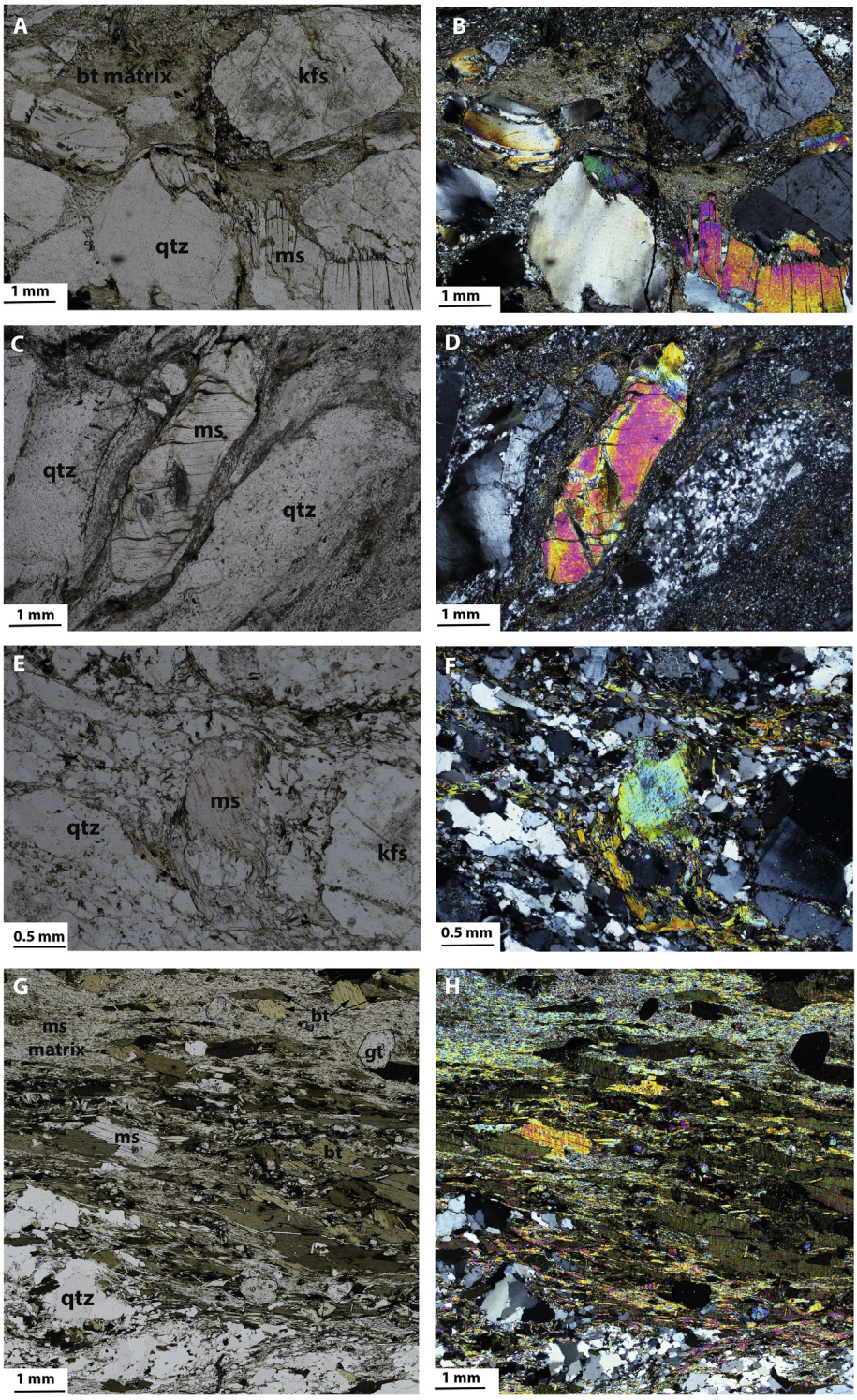

Fig. 3. Plane polarized light and crossed polar photomicrographs of typical mica crystals from the host granites and mylonite zones in the Collins Fault area. All samples yielded a Neoproterozoic age with the exception of GSWA 195890D (images C and D) which yielded a Paleoproterozoic age. A–D. Sample GSWA195890B (A and B) and 195890D (C and D) (3) a porphyritic muscovite–biotite metamonzogranite shows well preserved primary igneous muscovite surrounded by a finer grained matrix of biotite and quartz. E and F. Sample GSWA 216540B (2) a deformed metamonzogranite shows minimal preservation of primary igneous textures with recrystallised muscovite defining the main foliation. G–H. Sample GSWA 216,533 (1) a garnet–biotite gneiss defined by alternating layers of recrystallised quartz, tabular biotite and muscovite and recrystallised muscovite. ms = muscovite, bt = biotite, kfs = K-feldspar, qtz = quartz, gt = garnet. Numbers in brackets refer to locations in Fig. 1.

2011) was used and I22 included a fully calibrated WA1ms standard, which has an age of 2613 Ma (± 0.09%; Jourdan et al., 2014). The detailed analytical methodology is provided in Appendix A.

The mean J-value (irradiation parameter) computed from standard grains within the small pits was 0.01055740 ± 00000792 (± 0.075% 1 sigma) for the samples in irradiation I22 and 0.01085900 ± 00001466 (± 0.135% 1 sigma) for the samples in irradiation I23. Mass discrimination was monitored regularly through the analysis using an automated air pipette and provided a mean value of 1.00431 (± 0.04%) per dalton (atomic mass unit) relative to an air ratio of 298.56 ± 0.31 (Lee et al., 2006) for I22 and 1.003996 (± 0.06%) per dalton (atomic mass unit) relative to an air ratio of 298.56 ± 0.31 (Lee et al., 2006) for I23. The correction factors for interfering isotopes were $(^{39}Ar/^{37}Ar)_{Ca} = 7.0 \times 10^{-4}$ (± 1.2%), $(^{36}Ar/^{37}Ar)_{Ca} = 2.6 \times 10^{-4}$ (± 0.4%) and $(^{40}Ar/^{39}Ar)_{K} = 7.3 \times 10^{-4}$ (± 12.4%).

The criteria for the determination of plateaus are as follows: a plateau must include at least 70% of ^{39}Ar and the plateau should be distributed over a minimum of three consecutive steps agreeing at 95% confidence level and satisfying a probability of fit, or P-value, (P) of at

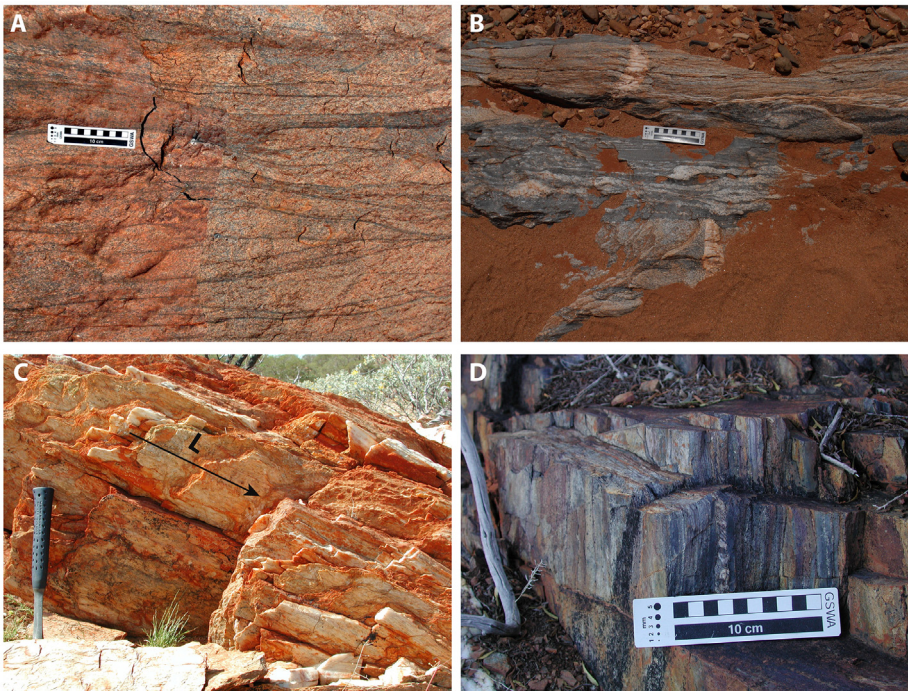

Fig. 4. A. Collins Fault outcrop showing anastomosing zones of 1–50 mm-wide mylonite within medium- to coarse-grained granitic rocks, GSWA 216540B (2). B. Compositionally weaker biotite–garnet schist (1) enclave within medium- to coarse-grained granitic rocks ~0.8 km west of the Collins Fault, GSWA 216533. C. ~5 m quartz mylonites (4) developed in granites with shallow plunging lineations from the central Gascoyne Province, GSWA 183294. D. Outcrop of a strongly foliated mudstone tending to chert (Edmund Group) (6) at the Ti Tree Shear Zone, GSWA 149010. Numbers in brackets refer to locations in Fig. 1 in the main body text.

least 0.05 (e.g., Jourdan et al., 2005). Mini-plateaus follow the same criteria except that they include between 50% and 70% of released ^{39}Ar and, as a consequence, are considered less reliable. Uncertainties include analytical and J-value errors. Plateau and mini-plateau ages from step-heated single-grain aliquots are reported with 2 sigma uncertainties.

4.2. SHRIMP U–Pb xenotime geochronology

Two samples were analysed using *in situ* U-Pb xenotime geochronology. Optical microscopy and scanning electron microscopy were used to identify suitable xenotime crystals (> 15 µm in diameter) for analysis by Sensitive High Resolution Ion Microprobe (SHRIMP). Xenotime grains > 15 µm across were drilled out in 3 mm-diameter plugs and cast in a single 25 mm epoxy mount. Xenotime reference materials were in a separate mount that was cleaned and Au-coated with the sample mounts prior to analysis.

The U-Pb data were obtained during two SHRIMP analytical sessions on the 13th and 20th October 2008. An O_2^- primary beam, with a spot size of 10–15 µm, was focussed through a 30 µm Kohler aperture with a beam intensity of 0.22–0.28nA. The secondary ion beam was focused through a 100-µm collector slit onto an electron multiplier to produce mass peaks with flat tops and a mass resolution (1% peak heights) of > 5000. A post-collector retardation lens was used to reduce stray ion produced from background counts. Xenotime was analysed with a 9-peak run table, and analytical procedures followed established methodologies (Fletcher et al., 2000, 2004). The primary Pb/U standard MG-1 ($^{206}Pb/^{238}U$ age of 490 Ma, $^{207}Pb/^{206}Pb$ age of 491.8 Ma, and U concentration of 1050 ppm) (Fletcher et al., 2004) was used for Pb/U, Pb/Th, and U and Th abundance calibrations. The secondary standards were z6413 (XENO1 of Stern and Rainbird, 2001) and BS-1 (Fletcher et al., 2004) used in conjunction with MG-1 for matrix corrections to Pb/U and Pb/Th. Z6413 was also used to monitor (and if necessary to correct) instrumental mass fractionation in $^{207}Pb/^{206}Pb$.

Squid-2.50.11.02.03 software (Ludwig, 2009) was used for initial data reduction, including correction for common Pb. Common Pb corrections were based on individual measured ^{204}Pb abundances and assuming crustal common Pb at the approximate age of the samples modelled by Stacey and Kramers (1975). Corrections for matrix effects in Pb/U and Pb/Th, and for instrumental mass fractionation in $^{207}Pb/^{206}Pb$, were carried out following established protocols as described by Fletcher et al. (2004). Weighted mean dates are reported with 95% confidence limits, whereas individual analyses are presented with 1 sigma uncertainties.

5. Geochronology results

5.1. $^{40}Ar/^{39}Ar$ mica age data

Single-grain muscovite from a mylonite sample at the Collins Fault (GSWA 216540B) yielded a plateau age of 898 ± 3 Ma (mini-plateau) (mean square weighted deviation (MSWD) = 1.07, P = 0.38). Single-grain muscovite and biotite from a biotite-garnet gneiss (GSWA 216533), ~0.8 km west of the Collins Fault, yielded plateau ages of, respectively, 918 ± 3 Ma (MSWD = 1.44, P = 0.13) and 908 ± 3 Ma (MSWD = 1.35, P = 0.24). Single-grain biotite from a mylonite ~ 2 km west of the Collins Fault (GSWA 195890B), yielded a plateau age of 862 ± 4 Ma (mini-plateau) (MSWD = 0.68, P = 0.64). However, muscovite from the same variably deformed outcrop sample yielded plateau ages of 1642 ± 7 Ma (MSWD = 1.72, P = 0.08) (GSWA 195890D) and 1639 ± 8 Ma (MSWD = 1.67, P = 0.08) (GSWA 195890E). Two quartz-mylonite samples from the centre of the orogen yielded muscovite plateau ages of 882 ± 3 Ma (MSWD = 1.19, P = 0.27) (183294) and 882 ± 3 Ma (MSWD = 0.67, P = 0.77) (GSWA 183295).

In summary, six plateau ages were calculated from our samples with > 70% ^{39}Ar released, and two 'mini-plateau' ages were calculated with > 50% ^{39}Ar (Figs. 5 and 6 and Table 2). The typical mica crystals seen in thin section from samples GSWA 195890B and D, 216533 and 216540B are shown in Fig. 3. However, since the analyses were completed on single grains from mineral separates it is not known whether the typical grains shown are the ones that were analysed.

5.2. U–Pb xenotime age data

Two xenotime crystals with distinct morphologies were identified in phyllite sample GSWA 149,009 from the Ti Tree Shear Zone: a 50 × 80 µm, anhedral crystal wrapped by the main foliation and a

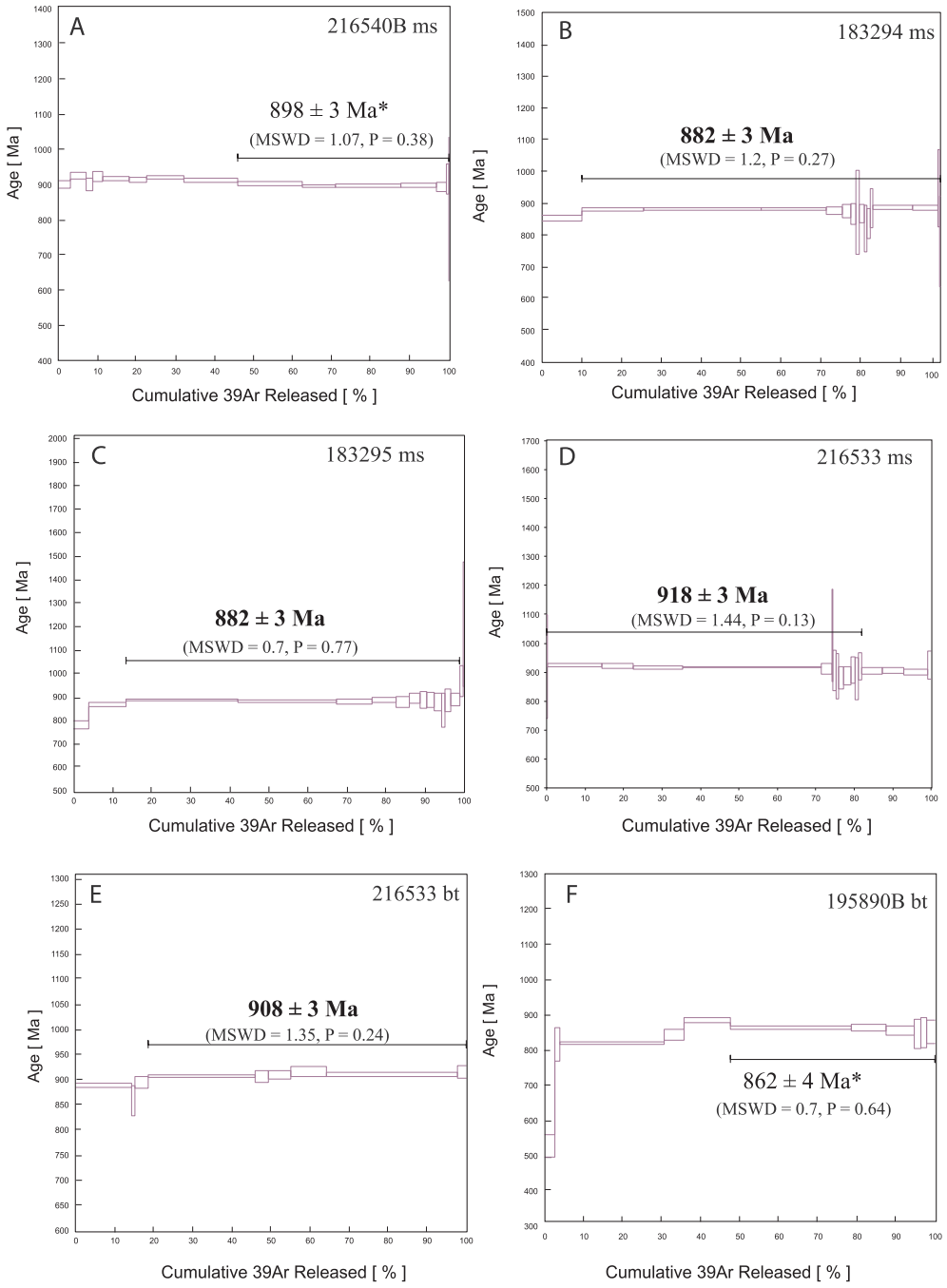

Fig. 5. A–F: $^{40}Ar/^{39}Ar$ age plateaus from mylonites within metagranites and quartz mylonites and a biotite schist from the Gascoyne Province. Asterisk indicates mini-plateau age determination. Mean ages are reported with 2 sigma uncertainty. ms = muscovite; bt = biotite.

subhedral crystal (~20 μm across) (Fig. 7A and B). Four analyses of the anhedral crystal yielded a weighted mean $^{207}Pb*/^{206}Pb*$ date of c. 1275 Ma and a single analysis on the subhedral crystal yielded a date of 891 ± 26 Ma (1σ) (Table 3). The second phyllite sample (GSWA 149010) contained elongate or subhedral xenotime crystals from ~30 to 90 μm in diameter (Fig. 7C–E). Seven analyses were carried out on five xenotime crystals (Table 3). Three statistical outliers (> 2 standard deviations from the mean) were excluded from the main group. The remaining four analyses yielded a weighted mean $^{207}Pb*/^{206}Pb*$ date of 887 ± 17 Ma (MSWD = 1.3) indistinguishable from the single analysis of 891 ± 26 Ma in the first sample. Combining the five analyses from the two samples yields a weighted mean $^{207}Pb*/^{206}Pb*$ date of 887 ± 9 Ma (MSWD = 0.96, n = 5) (Fig. 7F) interpreted as the age of hydrothermal xenotime growth.

6. Discussion

Our $^{40}Ar/^{39}Ar$ mica and U-Pb xenotime results of 918–862 Ma overlap with previously published total fusion $^{40}Ar/^{39}Ar$ mica dates of 960–820 Ma obtained from the Errabiddy Shear Zone in the southern Capricorn Orogen (Occhipinti and Reddy, 2009). In that study the authors interpreted their results as cooling ages related to the Edmundian Orogeny. Because mica argon dates in metamorphic terrains can either be interpreted as cooling ages (Scibiorski et al., 2015) or deformation ages (Hansma et al., 2016) we discuss the possibility of our data in terms of a new growth phase or cooling process. To assist with the interpretation we conducted diffusion modelling of muscovite. We integrate our new results with previously published geochronology to show that fault and shear zone reactivation spans not only the Gascoyne

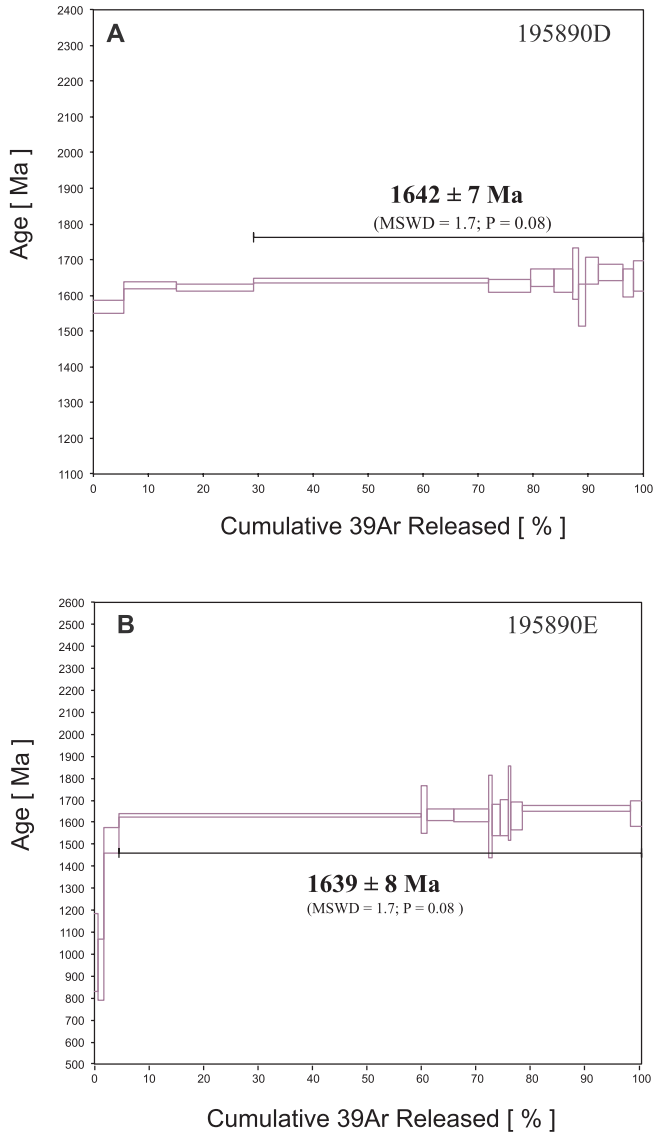

Fig. 6. A–B: $^{40}Ar/^{39}Ar$ muscovite age plateaus from a Paleoproterozoic metagranite from the Gascoyne Province. Mean ages are reported with 2 σ uncertainty.

Province but the bounding Archean cratons.

6.1. *$^{40}Ar/^{39}Ar$ diffusion modelling of muscovite from the northern Gascoyne Province*

Here we test whether the c. 900 Ma plateau ages are the result of complete thermal resetting of old muscovite (c. 1600 Ma) by regional thermal metamorphism or if they arose from the shear zone reactivation at c. 900 Ma. In the northern Capricorn Orogen, the observed crystal sizes in the shear zone are around 500 µm compared to the 4 mm c. 1640 Ma muscovite crystals (Fig. 3). Since the closure temperature of muscovite is proportional to the crystal (or more accurately domain) size, it is possible that the smaller crystals within the shear zone were reset by a regional Neoproterozoic thermal event whereas the larger crystals from the country rocks remained unaffected (e.g., Dunlap et al., 1991). Therefore, we carried out diffusion simulations on the effect of regional metamorphism on synthetic $^{40}Ar/^{39}Ar$ spectra using the ArArDiff algorithm (Jourdan and Eroglu, 2017). The modelling parameters included the selection of three grain sizes (in radius): 125 µm, 500 µm and 1000 µm (Table 4), each assumed to have resided in the same crustal volume at c. 900 Ma with an identical P–T history during the Neoproterozoic thermal event. The crystallisation age of the host rock was set at 1650 Ma, the known age of granitic rocks in the area (Sheppard et al., 2010b). It was assumed that the temperatures were ~150 °C either side of the Neoproterozoic thermal event period (they must have dropped below the muscovite closure temperature soon after igneous crystallisation since we obtained c. 1640 Ma plateau ages). The modelling comprised three time periods. Period 1 (920–880 Ma) involved heating from 150 °C up to an assumed peak of 420 °C, the minimum temperature needed to fully reset the small muscovite crystals for the duration used. Period 2 (880–860 Ma) involved cooling from the peak back to 150 °C. Period 3 (860–0 Ma) represents slow cooling as the rock was exhumed to its present-day location at the surface. The parameters used for the muscovite and the thermal events are listed in Table 4.

The diffusion modelling results show that the conditions needed to fully reset the smallest muscovite crystals (125 µm) at 920–860 Ma (100% ^{40}Ar loss) would also substantially affect the largest muscovite crystals. Muscovite with 500 µm and 1000 µm radius in our models have lost 52% and 26% of their $^{40}Ar*$ (relative to their Ar contents at 920 Ma immediately before the thermal event), effectively preventing these crystals from yielding plateau or even mini-plateau ages (Fig. 8). Because our $^{40}Ar/^{39}Ar$ analyses show that the larger muscovite crystals from the surrounding country rocks do not display strong diffusion patterns but rather yield well-defined plateau ages (Fig. 6), we conclude that it is unlikely that there was a regional thermal event at c. 900 Ma exceeding the muscovite closure temperature. Alternatively, it could be that the processes responsible for the c. 900 Ma muscovite ages were restricted to within the shear zones (i.e., sample 216540B which yielded 898 ± 3 Ma) whereas muscovite in the host granite was largely unaffected by this Neoproterozoic event (i.e., samples GSWA195890D and E which yielded 1642 ± 7 Ma and 1639 ± 8 Ma, respectively). As a consequence, our results suggest that either conditions within the shear zone (Collins Fault) were above the closure temperature (~450 °C) at c. 900 Ma but were much lower temperature away from the shear zone, or that regional temperatures were below the closure temperature across the entire northern Capricorn Orogen during

Table 2
$^{40}Ar/^{39}Ar$ muscovite and biotite results from the Gascoyne Province, Capricorn Orogen.

Sample ID	Mineral	Optical properties	Size Fraction (µm)	Plateau Age (Ma ± 2σ)	^{39}Ar (%)	MSWD	*P*	*n*
GSWA 183294	Muscovite	Aggregates of mica, yellowish color	< 355 > 212	882 ± 3	90.02	1.19	0.27	15
GSWA 183295	Muscovite	Sericitized, opaque and translucent	< 212 > 125	882 ± 3	85.49	0.67	0.77	12
GSWA 195890B	Biotite	Mostly unaltered and fresh	< 250 > 125	862 ± 4*	52.40	0.68	0.64	6
GSWA 216540B	Muscovite	Transparent, pearly luster	< 355 > 212	898 ± 3*	54.28	1.07	0.38	7
GSWA 216533	Biotite	Unaltered and fresh	< 355 > 212	908 ± 3	81.55	1.35	0.24	6
GSWA 216533	Muscovite	Transparent, pearly luster	< 355 > 212	918 ± 3	82.01	1.44	0.13	14
GSWA 195890D	Muscovite	Transparent, pearly luster	< 355 > 212	1642 ± 7	70.93	1.72	0.08	10
GSWA 195890E	Muscovite	Transparent, pearly luster	< 212 > 125	1639 ± 8	95.60	1.67	0.08	11

Notes: * indicates mini-plateau age determination (weighted mean age includes 50–70% of total ^{39}Ar.
MSWD, mean squared weighted deviation; P, P-value; n, number of steps used in plateau.

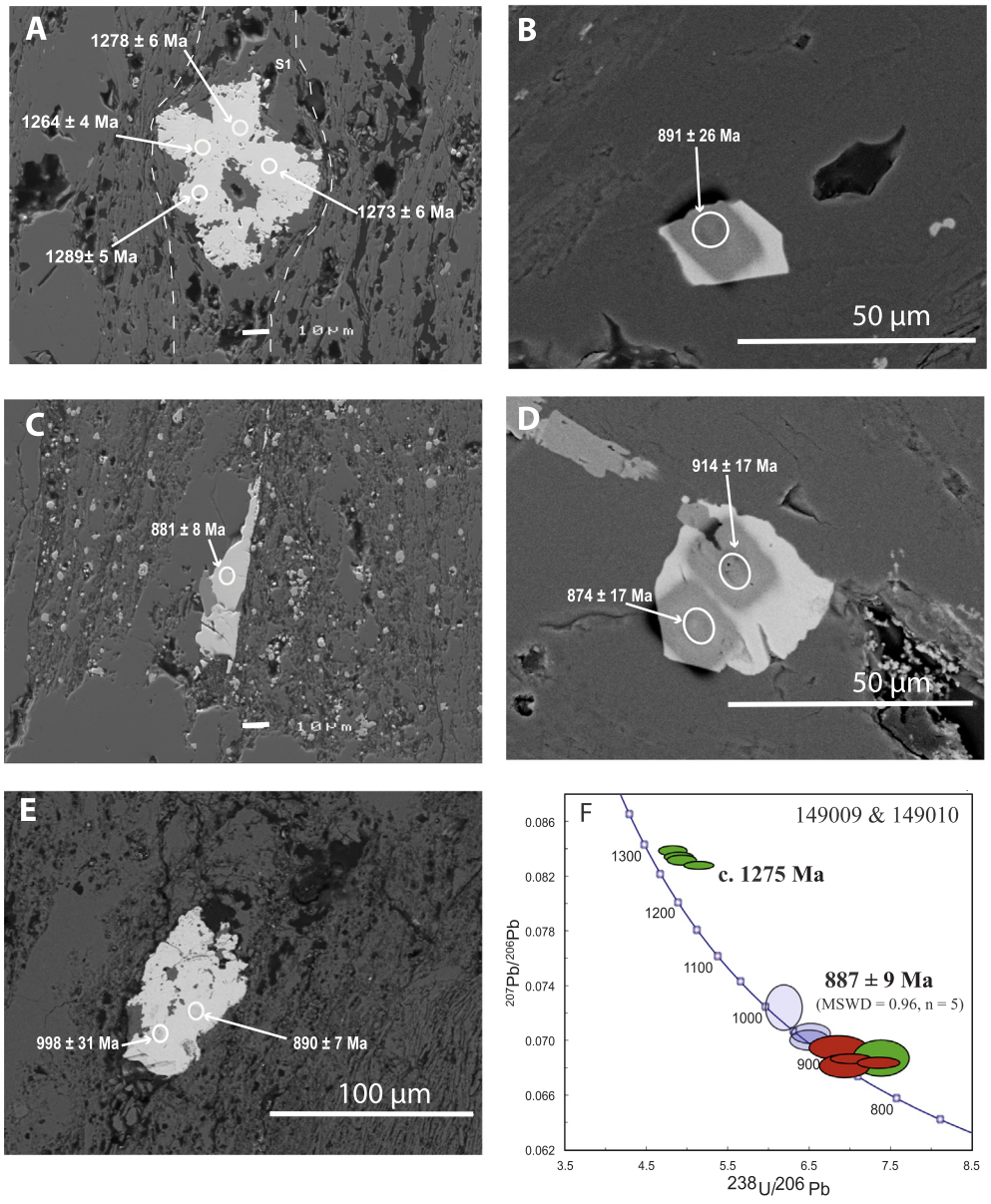

Fig. 7. A–E: Representative backscattered electron images of xenotime from siltstone/mudstone samples. A: Anhedral crystal wrapped by the 1.3–1.2 Ga quartz tectonic fabric (sample 149009). B: euhedral 25 µm xenotime crystal in quartz (Sample 149009). C: Euhedral to subhedral elongate and tabular xenotime crystal growing parallel to the adjacent quartz crystal (sample 149010) with intergrown Fe-oxide. D and E: Subhedral xenotime crystals with intergrowths and/or inclusions of Fe-oxides. F: Combined SHRIMP U-Pb xenotime results from samples 149,009 and 149010. Green ellipses denote analyses from sample 149009, red ellipses denote analyses from sample 149010, and transparent blue ellipses indicate statistical outliers excluded from the final weighted mean age calculation. Mean ages are quoted with 95% uncertainty intervals. (For interpretation of the references to color in this figure legend, the reader is referred to the web version of this article.)

Neoproterozoic reactivation, and the c. 900 Ma muscovite in the shear zone either grew or recrystallised at this time.

6.2. Ages of mica growth or cooling?

Current estimates of the closure temperature for muscovite and biotite are, respectively, ~425 ± 70 °C and ~365 ± 35 °C (Harrison et al., 1985, 2009; recalculated by Scibiorski et al. (2015). However, there are caveats on closure temperatures which include the following variables: grain size (a reduction in grain size typically causes a reduction in closure temperature: Dodson, 1973); the rate of cooling (faster cooling rates yield higher closure temperatures: Reddy and Potts, 1999) and; temperature of deformation (in particular, greenschist facies deformation commonly causes a reduction in grain size: Dunlap et al., 1991).

Our new $^{40}Ar/^{39}Ar$ results from low-grade mylonite zones could be interpreted as ages of mica neocrystallisation or recrystallisation (i.e., reduction in grain size). Determining whether the dates represent neocrystallisation ages can be difficult to ascertain, mainly because our study involve whole-grain analysis of mineral separates, which means the ages obtained cannot be readily linked to any microstructural observations or compositional data, unlike studies that use *in situ* laser argon analysis (e.g., Mulch and Cosca, 2004; Reddy et al., 1997). However, several mica $^{40}Ar/^{39}Ar$ studies on low-grade greenschist facies mylonite zones have demonstrated mica dates as neocrystallisation ages rather than cooling ages (e.g., Kirschner et al., 1996; Dunlap 1997).

Aggregates of muscovite within the mylonite zone at the Collins Fault (e.g., GSWA 216540B), form a well-defined foliation (Fig. 3E–F). In contrast, the Paleoproterozoic host rock sample away from the Collins Fault (GSWA 195890) consists of preserved igneous muscovite (as deformed porphyroclasts) and a foliation defined by very fine-grained biotite (Fig. 3A–D). The sizes of muscovite crystals in the shear zone have been significantly reduced compared with the large igneous muscovite crystals preserved in the host granite. The reduction in size is likely associated with low-grade deformation localised within the shear zone (Dunlap et al., 1991). In contrast, there appears to have been no new muscovite growth in the host rock away from the shear zone (sample GSWA 195890) as the muscovite yielded a Paleoproterozoic age.

Alternatively, our $^{40}Ar/^{39}Ar$ dates could be interpreted as cooling ages, an interpretation that would be consistent with that of Occhipinti

Table 3
SHRIMP U-Pb xenotime data from phyllite samples central Gascoyne Province, Capricorn Orogen.

Grain	Sample	$^{238}U^{\wedge}$	$^{232}Th^{\wedge}$	^{232}Th	f_{206}	$^{238}U/^{206}Pb^*$		$^{207}Pb^*/^{206}Pb^*$		$^{208}Pb^*/^{232}Th$		Disc	$^{238}U/^{206}Pb^*$		$^{207}Pb^*/^{206}Pb^*$	
.spot		(ppm)	(ppm)	$/^{238}U$	(%)	± 1 s		± 1 s		± 1 s		(%)	date (Ma) ± 1 s		date (Ma) ± 1 s	
Older group																
0812E.1-3	149,009	3878	2469	0.6	0.0103	4.8242	0.1156	0.0838	0.0628	0.0094	0.0002	6	1214	26	1289	5
0812E.1-1	149,009	4058	2882	0.7	0.0058	4.9006	0.1176	0.0834	0.0624	0.0094	0.0002	6	1197	26	1278	6
0812E.1-2	149,009	3668	1633	0.4	0.0114	4.9355	0.1177	0.0832	0.0619	0.0093	0.0002	7	1189	26	1273	6
0812E.1-4	149,009	4340	3205	0.7	0.0077	5.1491	0.1244	0.0828	0.0591	0.0091	0.0002	9	1144	25	1264	4
Main group																
0729G.1-1	149,010	3135	1356	0.4	0.0327	6.8584	0.2335	0.0695	0.0476	0.0096	0.0006	4	877	28	914	17
0729E.1-1	149,009	2144	1423	0.7	0.1163	7.3884	0.2262	0.0688	0.0425	0.0092	0.0009	8	818	23	891	26
0812 J.1-2	149,010	3810	1077	0.3	0.0087	7.0170	0.1664	0.0687	0.0455	0.0097	0.0002	3	859	19	890	7
0812 K.1-1	149,010	2862	842	0.3	0.0219	7.3555	0.1742	0.0684	0.0409	0.0093	0.0003	7	822	18	881	8
0729G.1-2	149,010	2910	771	0.3	0.0320	21.3637	4.5330	0.0682	0.0468	0.0099	0.0006	1	868	24	874	17
Statistical outliers																
0812 J.1-1	149,010	1275	1117	0.9	0.2765	6.1914	0.1481	0.0724	0.0521	0.0097	0.0011	3	965	21	998	31
0812D.1-1	149,010	1232	405	0.3	0.0553	21.0674	4.3294	0.0705	0.0475	0.0098	0.0005	2	920	21	943	14
0812B.1-1	149,010	1850	808	0.4	0.0618	6.5059	0.1568	0.0702	0.0476	0.0099	0.0004	1	922	21	935	13

Notes: ^Indicates measured ^{238}U and ^{232}Th levels. The precisions of ^{238}U and ^{232}Th abundances measured by SHRIMP are typically 5–10%.
Pb* indicates radiogenic Pb (i.e. corrected for common Pb).
f206, proportion of common ^{206}Pb in measured ^{206}Pb, determined using measured 204Pb/206Pb and contemporaneous common Pb composition (Stacey and Kramers, 1975)
Disc. is apparent discordance, as D (%) = 100 × ([$^{207}Pb^*/^{206}Pb^*$ date] − [$^{238}U/^{206}Pb^*$ date])/[$^{207}Pb^*/^{206}Pb^*$ date].
Analyses are sorted by descending $^{207}Pb^*/^{206}Pb^*$.

Table 4
Diffusion parameters and time-temperature history used in the ArArDiff models Jourdan and Eroglu (2017) to generate synthetic age spectra for muscovite.

Diffusion parameters					Mixed phases		
	D_0 (cm^2/s)	E_a (J/mol)	Radius (μm)	Modal composition	%K_2O for each mineral	K_2O contribution (mixed phase)	
Muscovite	2.30E + 00	264,000	125	1%	0.5%	33%	
Muscovite	2.30E + 00	264,000	500	44%	0.01%	33%	
Muscovite	2.30E + 00	264,000	1000	45%	0.01%	34%	
Thermal history							
	Crystallization age =	1650	Ma				
		Start (Ma)	End (Ma)	Duration (Ma)	Starting temp. (°C)	Ending temp. (°C)	Cooling rate (°C/Ma)
Period 1		920	880	40	150	470	−8
Period 2		880	860	20	470	150	16
Period 3		860	0	860	150	0	0
Period 4		0	0	0	0	0	

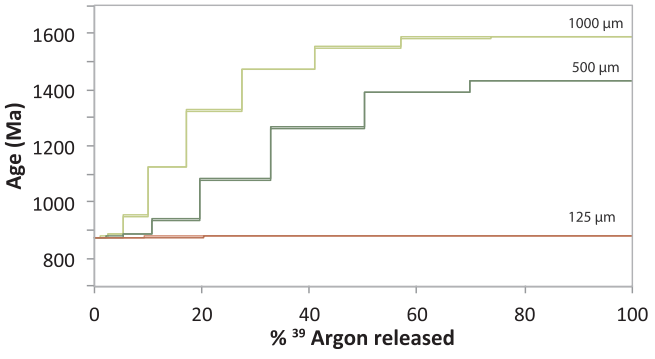

Fig. 8. Modelled $^{40}Ar/^{39}Ar$ age spectra for 125 μm, 500 μm and 1000 μm radius muscovite grains with an initial age of 1650 Ma that were later affected by a thermal overprint at 920–860 Ma that attained a maximum temperature of 460 °C (details of diffusion parameters and thermal history given in Table 4).

and Reddy (2009), who regarded their 960–820 Ma dates from the southern Errabiddy Shear Zone to represent cooling and uplift after the 1030–900 Ma Edmundian Orogeny. In particular, our mica (882 Ma) and xenotime (887 Ma) ages from the central parts of the province closely follow the end stages of reworking (c. 900 Ma) related to the Edmundian Orogeny. The xenotime interpreted as hydrothermal growth possibly formed during exhumation along the Ti Tree Shear Zone. Therefore, our mica dates from the quartz mylonites, immediately north of the Ti Tree Shear Zone, could also be related to the post-Edmundian cooling and exhumation. Here the lineations plunge at ~30° which indicates there was a component of dip-slip movement in addition to the predominant dextral strike-slip component.

In addition to our $^{40}Ar/^{39}Ar$ dates, there are four occurrences of 920–800 Ma U-Pb phosphate ages from faults zones within the Gascoyne Province and from the bounding Archean cratons: a xenotime date of 887 ± 9 Ma (this study) interpreted to represent new growth aided by hydrothermal fluids moving along the shear zone; monazite and xenotime dates at c. 920 Ma from the Chalba Shear Zone (Meadows et al., 2017) and; c. 850 Ma and c. 800 Ma phosphate dates, interpreted as growth from hydrothermal fluids moving along faults, from the adjacent Archean cratons (Rasmussen et al., 2007, 2010) (Fig. 9). The U–Pb phosphate ages demonstrate that there were fluids moving along pre-existing faults not only in the Gascoyne Province but within the bounding Archean cratons.

Our $^{40}Ar/^{39}Ar$ dates of 920–860 Ma could be interpreted as cooling ages, neocrystallization or recrystallization ages. However, the diffusion modelling and the petrographic evidence from the northern samples suggests that the 918–898 Ma ages represent mica growth. In contrast, interpretation of the younger muscovite dates (882 Ma), as either growth or cooling, from immediately north of the Ti Tree Shear

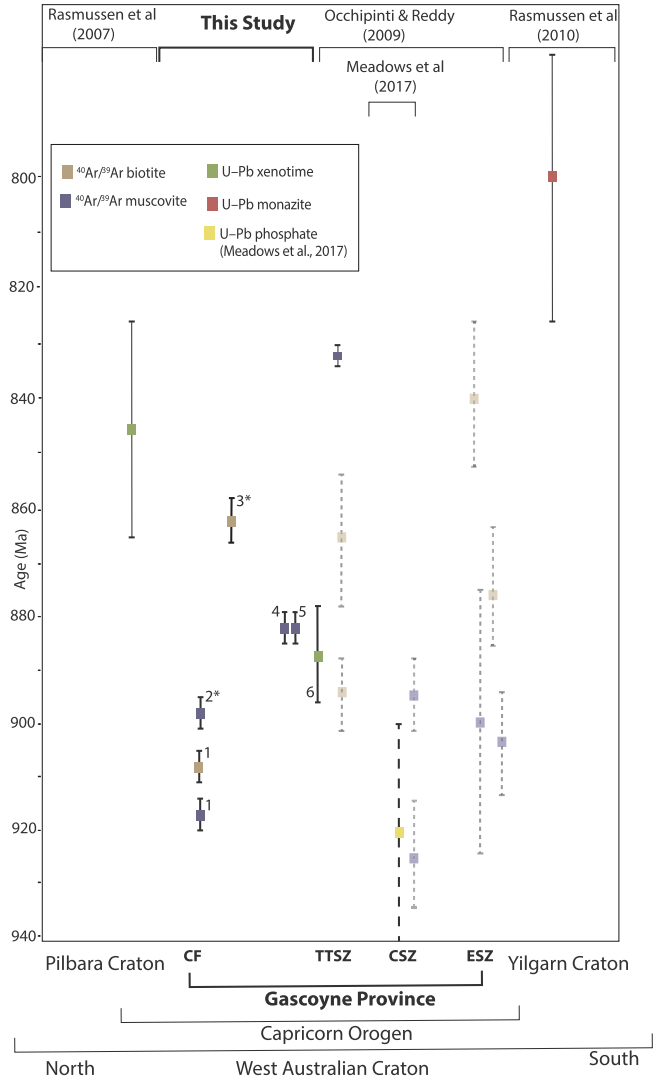

Fig. 9. Summary diagram illustrating the spread of ages defined by $^{40}Ar/^{39}Ar$ mica and SHRIMP U-Pb xenotime geochronology from major structures across the Gascoyne Province (this study) in comparison to published geochronology data in the province and from adjacent Archean Cratons. Only representative data from Occhipinti and Reddy (2009) are plotted. *Mini-plateau. (1) GSWA 216533; (2) GSWA 216540B; (3) GSWA 195890B; (4) GSWA 183294; (5) GSWA 183295; (6) GSWA 149,009 & 149101. ESZ—Errabiddy Shear Zone; CSZ—Chalba Shear Zone; —Ti Tree Shear Zone; CF—Collins Fault.

Zone remains equivocal.

6.3. The extent of the Neoproterozoic reactivation

Muscovite and biotite from greenschist facies mylonites and shear zones in c. 1680 Ma granitic rocks from the Collins Fault in the northern part of the Gascoyne Province yielded $^{40}Ar/^{39}Ar$ dates of 918 ± 3 Ma (muscovite, GSWA 216533), 908 ± 3 Ma (biotite, GSWA 216533) and 898 ± 3 Ma (muscovite mini-plateau age, GSWA 216540B). The muscovite dates are likely to be recording a growth phase for the reasons addressed above. Therefore, the estimated temperature during the reactivation must have been below ~425 ± 70 °C (the muscovite closure temperature, Scibiorski et al., 2015). Preliminary U–Pb monazite dating of samples GSWA 216,533 and GSWA 216540B yielded c. 1680 Ma ages (unpublished data). However, muscovite from mylonites in c. 1680 Ma granite ~2 km west of the Collins Fault, yielded dates of 1642 ± 7 Ma (GSWA 195890D) and 1639 ± 8 Ma (GSWA 195890E) and are interpreted as cooling ages of igneous muscovite that was unaffected by the Neoproterozoic reactivation event. However, biotite from the same rock (GSWA 195890B), forming the very fine-grained foliation, yielded a date of 862 ± 4 Ma (mini-plateau). This suggests that the temperature away from the main shear zone was either below or above 365 ± 35 °C (biotite closure temperature) but below 425 ± 70 °C (muscovite closure temperature).

Muscovite from two quartz-muscovite mylonites (GSWA 183,294 and 183295) 14 km apart in c. 1800 Ma granitic rocks (Minnie Creek batholith) farther south in the central part of the province, immediately north of the Ti Tree Shear Zone, both yielded $^{40}Ar/^{39}Ar$ dates of 882 ± 3 Ma. These shear zones also show dextral kinematics as seen in the north. This area north of the Ti Tree Shear Zone also was likely to have been uplifted at c. 1640 Ma because of the unconformable relationship between the 1680–1465 Ma Edmund Group sediments and the Minnie Creek batholith (Sheppard et al., 2010b). In contrast to the subhorizontal lineations in the northern part of the province here lineations plunge at 25–30° to the east-southeast which suggests there was some vertical component of movement in addition to the predominant dextral strike-slip component.

In contrast to the northern part of the province that displays consistent dextral movement along faults, the kinematics south of the Ti Tree Shear Zone are ambiguous. Our U-Pb xenotime age of 887 ± 9 Ma from the Ti Tree Shear Zone is interpreted to date hydrothermal fluids flow along the shear zone. This age overlaps with the youngest granite magmatism in this area at 899 ± 10 Ma (Piechocka et al., 2017) related to the Edmundian Orogeny. Our xenotime age may reflect growth during the uplift and exhumation during the later stages of the Edmundian Orogeny.

Our new dates overlap with poorly defined, total fusion $^{40}Ar/^{39}Ar$ mica error-dates of 925–820 Ma from the Errabiddy Shear Zone at the southern end of the Gascoyne Province (Occhipinti and Reddy, 2009). These dates were interpreted as approximate cooling ages related to a regional low-grade tectonic event associated with the Edmundian Orogeny (Occhipinti and Reddy, 2009). A single concordant plateau age of 832 ± 1.6 Ma came from a sample south of the Ti Tree Shear Zone (Fig. 1; Occhipinti and Reddy, 2009). Although many of their step-heated samples show signs of disturbance, the dataset does suggest that the Errabiddy Shear Zone was reactivated during the 920–860 Ma tectonism we have dated here. Furthermore, new U-Pb phosphate dates as young as c. 920 Ma suggest that Neoproterozoic activity also affected the Chalba Shear Zone (Meadows et al., 2017) (Fig. 9). Cutten et al. (2016) note that the 1680–1465 Ma Edmund and 1170–1070 Ma Collier Basins, present north of the Ti Tree Shear Zone are weakly metamorphosed. The Edmund Group may have been deformed either during the earlier 1320–1170 Ma Mutherbukin Tectonic Event or the Edmundian Orogeny whereas the younger Collier Group must have been affected during the Edmundian Orogeny or sometime later.

Outside of the core of the Capricorn Orogen, SHRIMP U-Pb *in situ* phosphate dates of c. 850 from the southern Pilbara Craton and 800 Ma from the northern Yilgarn Craton have been interpreted as precipitation from hydrothermal fluid flow along faults (Rasmussen et al., 2007, 2010). Their regional significance was unclear, but they could be related to discrete faulting and shearing in the margins of the bounding Archean cratons in response to the reactivation of faults in the Gascoyne Province dated here at 920–860 Ma (or 920–830 Ma if the single concordant plateau age of Occhipinti and Reddy (2009) is included as part of the same event). It is also likely that at least some faults in the 1170–1070 Ma Collier Basin formed at this time. This Neoproterozoic reactivation appears to overlap with and follow on directly from the 1030–900 Ma Edmundian Orogeny as previously defined. It seems unlikely that events spanning 1030–830 Ma would represent a tectonic continuum, but there are insufficient data at present to subdivide this history into a sequence of discrete tectonic events.

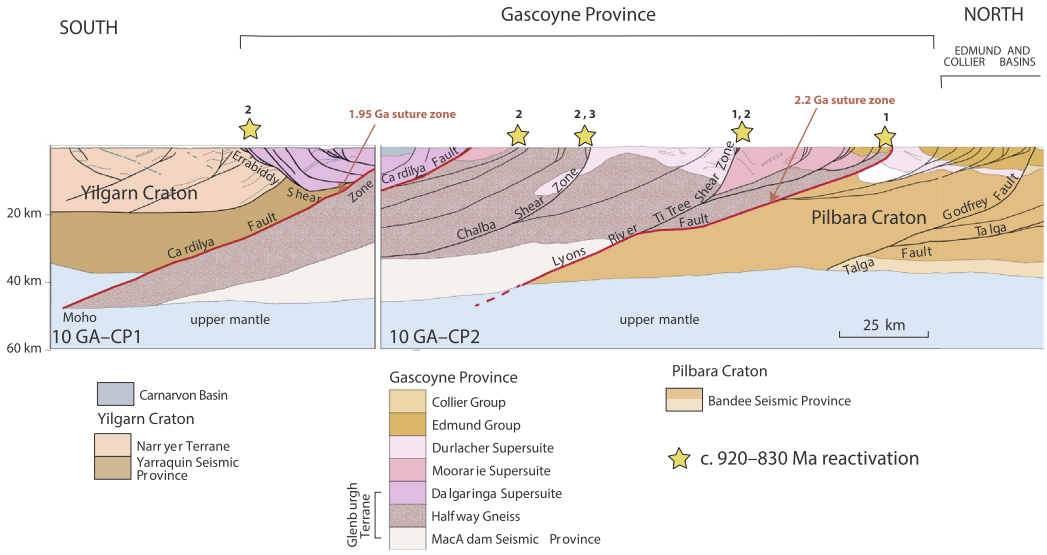

Fig. 10. Interpreted crustal geology from the seismic lines 10GHA–CP3 and 10GA–CP3 (Johnson et al., 2013) highlighting the crustal architecture dominated by south dipping mantle tapping faults and shear zones that were reactivated during the 920–830 Ma Neoproterozoic event. Refer to Fig. 1 for location of seismic line. (Modified from Johnson et al., 2013). 1: Reactivation dated in this study; 2: reactivation dated by Occhipinti and Reddy (2009); 3: reactivation dated by Meadows et al., (2017).

6.4. Implications of reactivation of pre-existing crustal sutures and faults

Our results, combined with existing data, show that Neoproterozoic reactivation affected the two former suture zones in the Capricorn Orogen: the 2200 Ma Collins Fault/Lyons River Fault and the 1950 Ma Errabiddy Shear Zone/Cardilya Fault (Occhipinti et al., 2004; Selway et al., 2009; Johnson et al., 2013), as well as other major crustal structures including the Ti Tree Shear Zone and the Chalba Shear Zone (Fig. 10). The Ti Tree Shear Zone is thought to have originated during Mesoproterozoic tectonism (Sheppard et al., 2010b) with recent evidence showing that the Ti Tree Shear Zone was active during the 1320–1170 Ma Mutherbukin Tectonic Event (Korhonen et al., 2017). The Neoproterozoic reactivation is best preserved within discrete structures whereas the adjacent low-grade greenschist rocks lack any distinct Neoproterozoic deformation fabrics (Sheppard et al., 2010b). This suggests that tectonism at this time was focussed within pre-existing structures.

Unlike the Petermann and Alice Springs orogenies in central Australia (Aitken et al., 2009) and the Tien Shan Orogen in central Asia (Raimondo et al., 2014), the lack of significant metamorphic discontinuities across Neoproterozoic shear zones in the Gascoyne Province and their preservation of subhorizontal lineations (at least in the north), suggest very little exhumation or crustal thickening during reactivation. However, we do see evidence for exhumation in the central parts of the province south of the Ti Tree Shear Zone with the juxtaposition of medium-grade rocks (formed during the Edmundian Orogeny) against low-grade metasedimentary rocks of the Edmund Group (Sheppard et al., 2010b).

In this study we have presented evidence for mica growth in the northern parts of the orogen related to dextral strike-slip reactivation. The interpretation of mica ages from the quartz–muscovite mylonites immediately north of the Ti Tree Shear Zone remains equivocal, but our U-Pb xenotime age from the Ti Tree Shear Zone could reflect phosphate growth during exhumation. This interpretation would be consistent with the cooling interpreted by Occhipinti and Reddy (2009). However, our field observations do not support the earlier interpretation of regional uplift of the orogen. Occhipinti and Reddy (2009) interpreted cooling ages of mica from the Gascoyne Province, together with Gascoyne-aged detrital zircon populations in Neoproterozoic Officer Basin to the east, to infer uplift and erosion of the western Capricorn Orogen. They suggested the cause of uplift to be collision of either Greater India or the Kalahari Craton with the West Australian Craton. However, our new geochronology data tied to dextral strike-slip kinematics of shear zones, in the northern parts of the province, along with the general lack of juxtaposition of rocks of substantially differing metamorphic grade, suggest there was no uplift in the northern part of the province. The structural interpretation of the deep seismic survey (Johnson et al., 2013) (Fig. 10) shows the boundary of the Pilbara Craton to extend at depth to the Ti Tree Shear Zone. Therefore, during north–south compression the southern part of the province may have been squeezed between the more rigid northern block and the Yilgarn Craton, which resulted in strike slip dextral faulting in the northern block and exhumation of the southern part of the orogen.

6.5. From reworking to reactivation on an orogen scale

An interesting finding of our study is that our $^{40}Ar/^{39}Ar$ mica and U–Pb xenotime dates from major shear zones and faults are only slightly younger than the youngest reworking event in the province (the 1030–900 Ma Edmundian Orogeny, Piechocka et al., 2017; Sheppard et al., 2007). The Edmundian Orogeny is largely restricted to a 20 km-wide zone in the central part of the province and is marked by greenschist to mid-amphibolite facies metamorphism and deformation. The intrusion of leucocratic granitic plutons and pegmatites in the centre of the orogen however post-dates the medium-grade reworking, which ceased at 990 Ma with magmatism having continued until 899 ± 10 Ma (Piechocka et al., 2017). The age for this youngest granitic rock is similar to our $^{207}Pb*/^{206}Pb*$ date of 887 ± 9 Ma for xenotime, interpreted as hydrothermal growth, from phyllites within the nearby Ti Tree Shear Zone, and to $^{40}Ar/^{39}Ar$ dates from across the Gascoyne Province recording reactivation. Therefore, from our new results and those of Piechocka et al. (2017), we show that while crustal reworking finished at 899 ± 10 Ma in the centre of the orogen (the youngest leucocratic magmatism) reactivation was occurring in the northern province at 918 ± 3 Ma. This records the transition from the final crustal reworking event in Capricorn Orogen to reactivation of crustal- and lithospheric-scale structures across the entire Gascoyne Province. Furthermore, the reworking history shows a pattern of

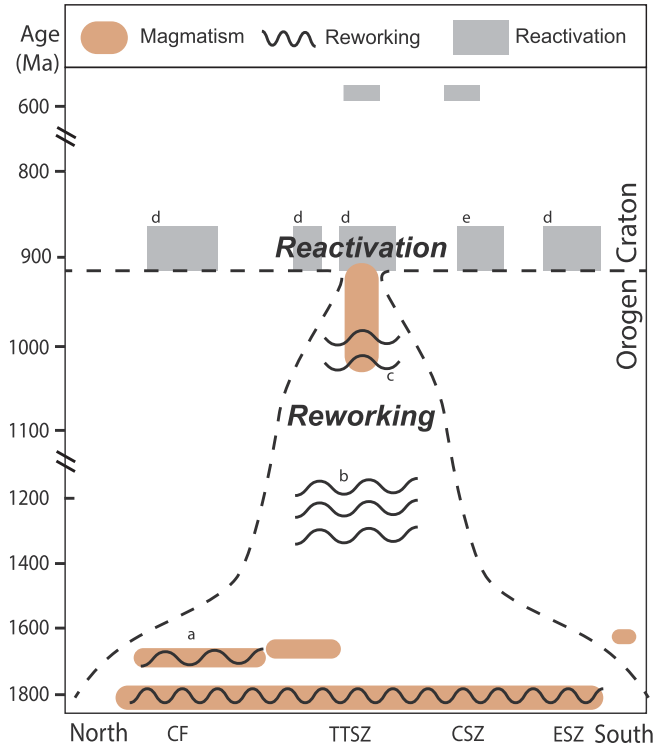

Fig. 11. Simplified time–space plot showing the distribution of reworking and reactivation events spanning the Gascoyne Province. [a] < 750 °C, > 6 kbar (Sheppard et al., 2005); [b] < 650 °C, 4.4–7 kbar (Korhonen and Johnson, 2015); [c]500–550 °C, 3–4 kbar (Sheppard et al., 2007), [d] < 350 °C (Occhipinti and Reddy 2009; this study), [e] > 640 °C, 3–4 kbar (Meadows et al., 2017). ESZ—Errabiddy Shear Zone; CSZ—Chalba Shear Zone; TTSZ—Ti Tree Shear Zone; CF—Collins Fault.

progressive narrowing of (medium and high-grade) reworking toward the centre of the orogen (Fig. 11) as the crust became more dehydrated and refractory (Korhonen and Johnson, 2015; Johnson et al., 2017).

Our results, which combine multi-mineral geochronology techniques and field observations, demonstrate how a long-lived orogen with a complex and protracted reworking history saw a breakout in fault reactivation across the Gascoyne Province at 920–860 Ma. The footprint of the c. 920–820 Ma Neoproterozoic activity (including the one concordant plateau age from Occhipinti and Reddy (2009)) extends across much of the West Australian Craton suggesting that the far-field forces responsible reflected tectonism on a much larger scale.

7. Conclusions

Our geochronology has identified Neoproterozoic mica dates of 918–862 Ma from shear zones in the northern Gascoyne Province. In the centre of the province we obtained mica dates of 882 Ma and a U-Pb xenotime age of 887 Ma. Argon diffusion modelling and field observations suggest the muscovite ages in the north reflect growth (neocrystallisation or crystallisation) ages during dextral strike-slip reactivation related to the Edmundian Orogeny. We find no evidence of exhumation of the northern parts of the province, but our interpretation of exhumation in the south is consistent with that of Occhipinti and Reddy (2009). However, rather than uplift due to a collision from the west, tectonism may have been caused by north–south compression resulting in a rigid northern block squeezing a less competent piece of crust between the Pilbara and Yilgarn Cratons. Our results suggest that the crustal architecture of the Capricorn Orogen was effectively frozen at c. 900 Ma, with only minor localised subsequent fault-related activity recorded. The lack of evidence for any younger significant regional tectonic events suggests that the structural architecture established during the Neoproterozoic reactivation event has essentially remained unchanged since then. Nevertheless, some of the structures that were active in the Neoproterozoic continue to be the focus of present-day seismicity (the Middalya and Mount Clere clusters in Fig. 2 of Revets et al., 2009; Keep et al., 2012).

Acknowledgments

The authors thank R. Parrish for constructive comments which have resulted in a more focussed and improved manuscript. C. Mayers of WAAIF is thanked for assistance during sample preparation. $^{40}Ar/^{39}Ar$ measurements were conducted at the Western Australian Argo Facility (WAAIF) and U–Th–Pb measurements were conducted using the SHRIMP ion microprobes, at the John de Laeter Centre at Curtin University, Western Australia. Simon Johnson publishes with permission of the Director of the Geological Survey of Western Australia. This PhD project was funded through an Australian Research Council (ARC) grant (LP130100922) and the Exploration Incentive Scheme.

Appendix A: Detailed analytical methods for $^{40}Ar/^{39}Ar$ geochronology

Irradiation 22: Twenty-four muscovite grains from sample 195890D were hand-picked from the < 355 µm > 212 µm fraction of which 12 were transparent with a pearly luster and chosen for irradiation. Sample 195890E yielded 30 grains from the < 212 µm > 125 µm fraction of which 25 were transparent with a pearly luster and chosen for irradiation.

Irradiation 23: Thirty muscovite grains from sample 216540B were hand-picked from the < 355 µm > 212 µm fractions and were transparent with a pearly luster. Sample 183294 hosted muscovite grains that were aggregates of mica with a distinct yellowish color, a total of 65 grains were picked from the < 355 µm > 212 µm fractions. Sample 183,295 yielded sericitized, opaque and translucent muscovite either intergrown with quartz (at the < 212 µm fraction) or free flaky mica at the > 125 µm fraction. Biotite from sample 216,533 was unaltered and fresh and 40 grains were picked at the < 355 µm > 212 µm fractions. Forty biotite crystals from sample 195890B were picked from the < 250 µm > 125 µm fractions.

For both irradiations the best grains the selected grains were loaded into discs and were irradiated for 40 h in the Oregon State University nuclear reactor in central position. The discs included a fully intercalibrated FCs standard, for which an age of 28.294 ± 0.037 Ma (± 0.13%; Renne et al., 2011) was used in I23 and a fully calibrated WA1ms standard, for which age of 2613 Ma ± 0.037 Ma (± 0.09%; Jourdan et al., 2014), used in I22. The discs were Cd-shielded (to minimize undesirable nuclear interference reactions) and irradiated in the Oregon State university nuclear reactor (USA) in central position.

For irradiation 22 the mean J-value computed from standard grains within the small pits yielded 0.01055740 ± 00000792 (± 0.075% 1 sigma) for the samples. Mass discrimination was monitored regularly through the analysis using an automated air pipette and provided a mean value of 1.00431 (± 0.04%) per dalton (atomic mass unit) relative to an air ratio of 298.56 ± 0.31 (Lee et al., 2006) The correction factors for interfering isotopes were $(^{39}Ar/^{37}Ar)_{Ca} = 7.0 \times 10^{-4}$ (± 1.2%), $(^{36}Ar/^{37}Ar)_{Ca} = 2.6 \times 10^{-4}$ (± 0.4%) and $(^{40}Ar/^{39}Ar)_{K} = 7.3 \times 10^{-4}$ (± 12.4%).

For irradiation 23 the mean J-value computed from standard grains within the small pits yielded 0.01085900 ± 00001466 (± 0.135% 1 sigma) for the samples. Mass discrimination was monitored regularly through the analysis using an automated air pipette and provided a mean value of 1.003996 (± 0.06%) per dalton (atomic mass unit) relative to an air ratio of 298.56 ± 0.31 (Lee et al., 2006). The correction factors for interfering isotopes were $(^{39}Ar/^{37}Ar)_{Ca} = 7.0 \times 10^{-4}$ (± 1.3%), $(^{36}Ar/^{37}Ar)_{Ca} = 2.7 \times 10^{-4}$ (± 0.84%) and $(^{40}Ar/^{39}Ar)_{K} = 7.3 \times 10^{-4}$ (± 12.4%).

During both analytical sessions muscovite and biotite were step-heated using a 110 W Spectron Laser Systems, with a continuous Nd-YAG (IR; 1064 nm) laser rastered over the sample during 1 min to ensure an homogenously distributed temperature. The gas was purified in a stainless steel extraction line using two SAES AP10 getters and a GP50 getter. Ar isotopes were measured in static mode using a MAP 215–50 mass spectrometer (resolution of ~450; sensitivity of 4×10^{-14} mol/V) with a Balzers SEV 217 electron multiplier using 9 to 10 cycles of peak-hopping. The data acquisition was performed with the Argus program written by M.O. McWilliams and ran under a LabView environment. Blanks were monitored every 3–4 steps and typical ^{40}Ar blanks range from 1×10^{-16} to 2×10^{-16} mol. The raw data were processed using the ArArCALC software (Koppers, 2002) and the ages have been calculated using the decay constants recommended by Renne et al. (2011). Blanks were monitored every 3–4 steps. All parameters and relative abundance values are provided in Supplementary Tables DR S1–6 (a separate file for each sample is attached as an excel spreadsheet) and have been corrected for blank, mass discrimination and radioactive decay. Individual errors in Supplementary Tables DR S2–7 are given at the 1σ level.

The criteria for the determination of plateau are as follows: plateaus must include at least 70% of ^{39}Ar. The plateau should be distributed over a minimum of 3 consecutive steps agreeing at 95% confidence level and satisfying a probability of fit (P) of at least 0.05 (e.g., Jourdan et al., 2005). Mini-plateaus follow the same criteria except that they include between 50% and 70% ^{39}Ar released and are considered less reliable. Uncertainties include analytical and J-value errors. All sources of uncertainties are included in the calculations.

Appendix B. Supplementary data

Supplementary data associated with this article can be found, in the online version, at http://dx.doi.org/10.1016/j.precamres.2018.04.006.

References

Aitken, A.R.A., Betts, P.G., Ailleres, L., 2009. The architecture, kinematics, and lithospheric processes of a compressional intraplate orogen occurring under Gondwana assembly: the Petermann orogeny, central Australia. Lithosphere 6, 343–357. http://dx.doi.org/10.1130/L39.1.

Aitken, A.R.A., Raimondo, T., Capitanio, F.A., 2013. The intraplate character of supercontinent tectonics. Gondwana Res. 24, 807–814. http://dx.doi.org/10.1016/j.gr.2013.03.005.

Bodorkos, S., Wingate, M.T.D., 2007. The contribution of geochronology to GSWA's mapping programs: current perspectives and future directions. Geol. Survey Western Austr. 2007 (2), 11.

Cawood, P.A., Tyler, I.M., 2004. Assembling and reactivating the Proterozoic Capricorn Orogen: lithotectonic elements, orogenies, and significance. Precambr. Res. 128, 201–218. http://dx.doi.org/10.1016/j.precamres.2003.09.001.

Cutten, H.N., Johnson, S.P., Thorne, A.M., Wingate, M.T.D., Kirkland, C.L., Belousova, E.A., Blay, O.A., Zwingmann, H., 2016. Deposition, provenance, inversion history and mineralization of the Proterozoic Edmund and Collier Basins, Capricorn Orogen. Geol. Survey Western Austr. Rep. 127, 80.

Dodson, M.H., 1973. Closure temperature in cooling geochronological and petrological systems. Contr. Mineral. Petrol. 40, 259–274. http://dx.doi.org/10.1007/BF00373790.

Dunlap, W.J., 1997. Neocrystallization or cooling? ^{40}Ar/^{39}Ar ages of white micas from low-grade mylonites. Chem. Geol. 143, 181–203. http://dx.doi.org/10.1016/S0009-2541(97)00113-7.

Dunlap, W., Teyssier, C., McDougall, I., Baldwin, S., 1991. Ages of deformation from K/Ar and ^{40}Ar/^{39}Ar dating of white micas. Geology 19, 1213–1216. http://dx.doi.org/10.1130/0091-7613(1991) 019<1213:AODFKA>2.3.CO;2.

Dyksterhuis, S., Müller, R.D., 2008. Cause and evolution of intraplate orogeny in Australia. Geology 36, 495–498. http://dx.doi.org/10.1130/G24536A.1.

Fletcher, I.R., McNaughton, N.J., Aleinikoff, J.A., Rasmussen, B., Kamo, S.L., 2004. Improved calibration procedures and new standards for U-Pb and Th-Pb dating of Phanerozoic xenotime by ion microprobe. Chem. Geol. 209, 295–314. http://dx.doi.org/10.1016/j.chemgeo.2004.06.015.

Fletcher, I.R., McNaughton, N.J., Rasmussen, B., 2000. SHRIMP U-Pb geochronology of authigenic xenotime and its potential for dating sedimentary basins. Austr. J. Earth Sci. 47, 845–859. http://dx.doi.org/10.1046/j.1440-0952.2000.00819.x.

Hanmer, S., Passchier, C.W., 1991. Shear sense indicators: a review. Geol. Survey Can. 90, 70.

Hansma, J., Tohver, E., Schrank, C., Jourdan, F., Adams, D., 2016. The timing of the Cape Orogeny: new 40Ar/39Ar age constraints on deformation and cooling of the Cape Fold Belt, South Africa. Gondwana Res. 32, 122–137. http://dx.doi.org/10.1016/j.gr.2015.02.005.

Harrison, T.M., Célérier, J., Aikman, A.B., Hermann, J., Heizler, M.T., 2009. Diffusion of ^{40}Ar in muscovite. Geochimica et Cosmochimica Acta 73, 1039–1051. http://dx.doi.org/10.1016/j.gca.2008.09.038.

Harrison, T.M., Duncan, I., McDougall, I., 1985. Diffusion of ^{40}Ar in biotite: temperature, pressure and compositional effects. Geochimica et Cosmochimica Acta 49, 2461–2468. http://dx.doi.org/10.1016//0016-7037(85)90246-7.

Johnson, S.P., Korhonen, F.J., Kirkland, C.L., Cliff, J.B., Belousova, E.A., Sheppard, S., 2017. An isotopic perspective on growth and differentiation of Proterozoic orogenic crust: from subduction magmatism to cratonization. Lithos 268, 76–86. http://dx.doi.org/10.1016/j.lithos.2016.11.003.

Johnson, S.P., Sheppard, S., Rasmussen, B., Wingate, M.T.D., Kirkland, C.L., Muhling, J.R., Fletcher, I.R., Belousova, E.A., 2011. Two collisions, two sutures: punctuated pre-1950 Ma assembly of the West Australian Craton during the Ophthalmian and Glenburgh Orogenies. Precambr. Res. 189, 239–262. http://dx.doi.org/10.1016/j.precamres.2011.07.011.

Johnson, S.P., Thorne, A.M., Tyler, I.M., Korsch, R.J., Kennett, B.L.N., Cutten, H.N., Goodwin, J., Blay, O., Blewett, R.S., Joly, A., Dentith, M.C., Aitken, A.R.A., Holzschuh, J., Salmon, M., Reading, A., Heinson, G., Boren, G., Ross, J., Costelloe, R.D., Fomin, T., 2013. Crustal architecture of the Capricorn Orogen, Western Australia and associated metallogeny. Austr. J. Earth Sci. 60, 681–705. http://dx.doi.org/10.1080/08120099.2013.826735.

Jourdan, F., Eroglu, E., 2017. ^{40}Ar/^{39}Ar and (U-Th)/He model age signatures of elusive mercurian and venusian meteorites. Meteoritics Planetary Sci.

Jourdan, F., Feraud, G., Bertrand, A.B., Kampunzu, G., Tshoso, M.K., Watkeys, B., 2005. Karoo large igneous province; brevity, origin, and relation to mass extinction questioned by new ^{40}Ar/^{39}Ar age data. Geology 33, 745–748. http://dx.doi.org/10.1130/G21632.1.

Jourdan, F., Frew, A., Joly, A., Mayers, C., Evans, N.J., 2014. WA1ms: A ~2.61 Ga muscovite standard for ^{40}Ar/^{39}Ar dating. Geochimica et Cosmochimica Acta 141, 113–126. http://dx.doi.org/10.1016/j.gca.2014.06.010.

Keep, M., Hengesh, J., Whitney, B., 2012. Natural seismicity and tectonic geomorphology reveal regional transpressive strain in northwestern Australia. Austr. J. Earth Sci. 59, 341–354. http://dx.doi.org/10.1080/08120099.2012.667439.

Kirschner, D.I., Cosca, M.A., Masson, H., Hunziker, C., 1996. Staircase 40/Ar39Ar spectra of fine-grained white mica: timing and duration of deformation and empirical constraints on argon diffusion. Geology 24, 747–750. http://dx.doi.org/10.1130/0091-7613(1996) 024<0747:SAASO F>2.3.CO;2.

Korhonen, F.J., Johnson, S.P., 2015. The role of radiogenic heat in prolonged intraplate reworking: the Capricorn Orogen explained? Earth Planetary Sci. Lett. 428, 22–32. http://dx.doi.org/10.1016/j.epsl.2015.06.039.

Korhonen, F.J., Johnson, S.P., Wingate, M.T.D., Kirkland, C.L., Fletcher, I.R., Dunkley, D.J., Roberts, M.P., Sheppard, S., Muhling, J.R., Rasmussen, B., 2017. Radiogenic heating and craton-margin plate stresses as drivers for intraplate orogeny. J. Metamorphic Geol. 35, 631–661. http://dx.doi.org/10.1111/jmg.12249.

Lee, Y.J., Marti, K., Severinghaus, J.P., Kawamura, K., Yoo, H.S., Lee, J.B., Kim, J.S., 2006. A redetermination of the isotopic abundances of atmospheric Ar. Geochimica et Cosmochimica Acta 70, 4507–4512 doi.org/10.1016/j.gca.2006.06.1563.

Ludwig, K.R., 2009. Squid 2.50, A User's Manual. Berkeley Geochronology Centre Special Publication, pp. 95.

Meadows, H.R., Reddy, S.M., Clark, C., Plavsa, D., Johnson, T., 2017. Localisation of High Strain and High Temperature into the Chalba Shear Zone. Specialist Group in Tectonics and Structural Geology, Gascoyne Province Conference Abstract.

Mulch, A., Cosca, M.A., 2004. Recrystallization or cooling ages: *in situ* UV-laser 40Ar/39Ar geochronology of muscovite in mylonitic rocks. J. Geol. Soc. 161, 573–582. http://dx.doi.org/10.1144/0016-764903-110.

Occhipinti, S.A., Reddy, S.M., 2009. Neoproterozoic reworking of the Paleoproterozoic Capricorn Orogen of Western Australia and implications for the amalgamation of Rodinia. Geol. Soc., London, Spec. Publ. 327, 445–456. http://dx.doi.org/10.1144/SP327.18.

Occhipinti, S.A., Sheppard, S., Passchier, C., Tyler, I.M., Nelson, D.R., 2004. Paleoproterozoic crustal accretion and collision in the southern Capricorn Orogen: the Glenburgh Orogeny. Precambr. Res. 128, 237–255. http://dx.doi.org/10.1016/j.precamres.2003.09.002.

Piechocka, A.M., Gregory, C.J., Zi, J., Sheppard, S., Wingate, M.T.D., Rasmussen, B., 2017. Monazite trumps zircon: applying SHRIMP U-Pb geochronology to systematically evaluate emplacement ages of leucocratic, low-temperature granites in a complex Precambrian orogen. Contr. Mineral. Petrol. 172, 1–17. http://dx.doi.org/10.1007/S00410-017-1386-5.

Raimondo, T., Hand, M., Collins, M.J., 2014. Compressional intracontinental orogens: ancient and modern perspectives. Earth-Sci. Rev. 130, 128–153. http://dx.doi.org/10.1016/j.earscirev.2013.11.009.

Raimondo, T., Collins, A.S., Hand, M., Walker-Hallam, A., Smithies, R.H., Evins, P.M., Howard, H.M., 2010. The anatomy of a deep intracontinental orogen. Tectonics 29, 1–31. http://dx.doi.org/10.1029/2009TC002504.

Rasmussen, B., Fletcher, I.R., Muhling, J.R., Thorne, W.S., Broadbent, G.C., 2007. Prolonged history of episodic fluid flow in giant hematite ore bodies: Evidence from *in situ* U-Pb geochronology of hydrothermal xenotime. Earth Planetary Sci. Lett. 258, 249–259. http://dx.doi.org/10.1016/j.epsl.2007.03.033.

Rasmussen, B., Fletcher, I.R., Muhling, J.R., Wilde, A.W., 2010. *In situ* U-Th–Pb geochronology of monazite and xenotime from the Jack Hills belt: Implications for the age of deposition and metamorphism of Hadean zircons. Precambr. Res. 180, 26–46. http://dx.doi.org/10.1016/j.precamres.2010.03.004.

Reddy, S.M., Kelley, S.P., Magennis, L., 1997. A microstructural and argon laserprobe study of shear zone development at the western margin of the Nanga Parbat-

Haramosh Massif, western Himalaya. Contri. Mineral. Petrol. 128, 16–29. http://dx.doi.org/10.1007/s004100050290.
Reddy, S.M., Occhipinti, S.A., 2004. High-strain zone deformation in the southern Capricorn Orogen, Western Australia: kinematics and age constraints. Precambr. Res. 128, 295–314. http://dx.doi.org/10.1016/j.precamres.2003.09.005.
Reddy, S.M., Potts, G.J., 1999. Constraining absolute deformation ages: the relationship between deformation mechanisms and isotope systematics. J. Struct. Geol. 21, 1255–1265. http://dx.doi.org/10.1016/S0191-8141(99)00032-2.
Renne, P.R., Balco, G., Ludwig, K.R., Mundil, R., K. Min,Response to the comment by W.H. Schwarz,, et al., 2011. on "Joint determination of 40K decay constants and 40Ar*/40K for the Fish Canyon sanidine standard, and improved accuracy for 40Ar/39Ar geochronology" by P. R. Renne et al. (2010). Geochim. Cosmochim. Acta 75, 5097–5100. http://dx.doi.org/10.1016/j.gca.2011.06.021.
Revets, S.A., Keep, M., Kennett, B.L.N., 2009. NW Australian intraplate seismicity and stress regime. J. Geophys. Res. 114, 1–10. http://dx.doi.org/10.1029/2008jb006152.
Scibiorski, E., Tohver, E., Jourdan, F., 2015. Rapid cooling and exhumation in the western part of the Mesoproterozoic Albany-Fraser Orogen, Western Australia. Precambr. Res. 265, 232–248. http://dx.doi.org/10.1016/j.precamres.2015.02.005.
Selway, K., Sheppard, S., Thorne, A.M., Johnson, S.P., Groenewald, P.B., 2009. Identifying the lithospheric structure of a Precambrian orogen using magneto-tellurics: The Capricorn Orogen, Western Australia. Precambr. Res. 168, 185–196. http://dx.doi.org/10.1016/j.precamres.2008.09.010.
Sheppard, S., Bodorkos, S., Johnson, S.P., Wingate, M.T.D., Kirkland, C.L., 2010a. The paleoproterozoic capricorn orogeny: intracontinental reworking not continent-continent collision. Geol. Survey Western Austr. 108, 33.
Sheppard, S., Johnson, S.P., Wingate, M.T.D., Kirkland, C.L., Pirajno, F., 2010b. Explanatory notes for the Gascoyne Province. Geological Survey of Western Australia 1:100 000 Explanatory Notes, pp.336.
Sheppard, S., Occhipinti, S.A., Nelson, D.R., 2005. Intracontinental reworking in the Capricorn Orogen, Western Australia: the 1680–1620 Ma Mangaroon Orogeny. Austr. J. Earth Sci. 52, 443–460. http://dx.doi.org/10.1080/08120090500134589.
Sheppard, S., Rasmussen, B., Muhling, J.R., Farrell, T.R., Fletcher, I.R., 2007. Grenvillian-aged orogenesis in the Palaeoproterozoic Gascoyne Complex, Western Australia: 1030–950 Ma reworking of the Proterozoic Capricorn Orogen. J. Metamorphic Geol. 25, 477–494. http://dx.doi.org/10.1111/j.1525-1314.2007.00708.x.
Stacey, J.S., Kramers, J.D., 1975. Approximation of terrestrial lead isotope evolution by a two-stage model. Earth Planetary Sci. Lett. 26, 207–221. http://dx.doi.org/10.1016/0012-821X(75)90088-6.
Stern, R.A., Rainbird, R.H., 2001. Advancements in Xenotime U–Pb Geochronology by ion Microprobe. Eleventh V.I. Goldschmidt Conference Lunar and Planetary Science Institute, Houston.
Wingate, M.T.D., Giddings, J.W., 2000. Age and palaeomagnetism of the Mundine Well dyke swarm, Western Australia: implications for an Australia-Laurentia connection at 755 Ma. Precambr. Res. 100, 335–357. http://dx.doi.org/10.1016/S0301-9268(99)00080-7.
Koppers, A. A. P., 2002, ArArCALC—Software for 40Ar/39Ar age calculations: Computers & Geoscienc, v. 28, p. 605–619, doi: 10.1016/S0098-3004(01)00095-4.